Optical second-harmonic scattering from cylindrical particles

Jerry Icban Dadap
Department of Applied Physics and Applied Mathematics, Columbia University, New York, New York 10027, USA
(Received 2 April 2008; revised manuscript received 15 July 2008; published 20 November 2008)

The theory of optical second-harmonic (SH) scattering from finite cylinders of arbitrary size, orientation, and crystallographic structure is developed within the Rayleigh-Gans-Debye approximation for plane-wave excitation. Both cases of particles comprised of noncentrosymmetric and centrosymmetric media are examined. For particles comprised of noncentrosymmetric media, all nonlinear susceptibility elements share a common "linear" scattering form factor. For centrosymmetric media, the various nonlinear susceptibility components arising from the surface response experience different scattering form factors. Regardless of the type of media, SH scattering from finite cylinders may be described in terms of an effective nonlinear susceptibility tensor for the particle. Several essential aspects of the SH scattering process are analyzed, such as the radiation patterns and their dependence on particle orientation and input polarization, its chiral response, as well as the size and wavelength scaling for small particles.

DOI: 10.1103/PhysRevB.78.205322 PACS number(s): 42.65.Ky, 78.35.+c, 82.70.Dd, 78.67.−n

I. INTRODUCTION

The application of second-order nonlinear optical techniques for investigating the structure and various properties of small particles, such as second-harmonic generation (SHG) and sum-frequency generation (SFG), is a subject of considerable current interest. SHG was already recognized as a probe of noncentrosymmetric particles as early as in the beginning of the 1960s. In that decade, SHG was developed and employed to classify particles according to the strength of their nonlinear response and their potential for phase matching.[1] Recently, SHG has been shown to permit inference of the crystallographic orientation of individual particles.[2–5] SHG is also a well-developed tool for investigating surfaces of materials possessing centrosymmetric media.[6–12] Such capability arises from the fact that, within the dipole approximation, SHG is forbidden from the bulk of a centrosymmetric medium but is allowed at the surface, where the inversion symmetry is broken. This property has been exploited to probe the surfaces of small spheres made of centrosymmetric material.[13] Recent reviews illustrate the increasing importance of the SHG/SFG techniques not only as probes of small particles,[14,15] but also as significant tools in nonlinear optical microscopy.[16–19]

Although the nonlinear response of a particle reflects its crystallographic symmetry, the shape of the particle plays an equally important role in defining the SH excitation and radiation processes.[20,21] For example, it has been shown theoretically[22,23] and experimentally[24,25] that in the Rayleigh limit, a small sphere comprised of a centrosymmetric medium radiates SH mainly via two modes: nonlocally excited electric-dipole and locally excited electric-quadrupole moments. Slight deviation from the spherical shape, however, may lead to a *locally* excited dipole moment, with radiation and polarization properties differing significantly from those of a sphere.[26,27] A recent theoretical study has further elucidated the relationship between the particle's structure and the SHG electromagnetic selection rules.[28] While second-order nonlinear optical experiments on nonspherical particles continue to grow at a rapid pace,[5,29–46] the theoretical description of second-order nonlinear optical scattering has been largely limited to spherical particles.[22,23,47–55]

We briefly describe some of the relevant prior theoretical studies of SH electromagnetic scattering from nonspherical particles. An early calculation of SHG from cylinders was carried out to explain SHG from collagen fibrils.[56,57] Recent works include the theory of SH scattering arising from (1) the surface of a two-dimensional structure of arbitrary[58] and circular[59] cross-sectional shape, (2) the bulk nonlocal response of an infinite wire of centrosymmetric medium,[60,61] and (3) the bulk local response of a nanowire of noncentrosymmetric medium supported by a metallic surface.[5] Related studies include SHG from plasmon excitation of two-dimensional metallic structures[62] and first-principles calculations of the nonlinear optical response of nanotubes.[63–65] The theoretical treatments of SH scattering described above are based on two-dimensional geometries, i.e., an infinitely long structure, with the fundamental excitation traveling along or transverse to the axis of this configuration. Despite these developments, SHG from cylinders of finite dimensions, arbitrary orientation, and arbitrary material symmetry has not been explored. The length of a cylindrical particle, for example, plays an important role in the SH scattering from such particles, as has been recently demonstrated.[44] Thus, we address the need for a theoretical description that provides basic understanding of the nonlinear response of finite anisotropic particles, as modeled by a cylinder of finite length.

Before extracting the nonlinear optical response of anisotropic structures, one needs to consider their linear optical response. For the general case of linear electromagnetic scattering from a finite cylinder having a different dielectric constant from that of its surrounding environment, there is no closed-form solution to Maxwell's equations.[66–68] Approximate solutions, however, exist when the refractive indices of the two media are nearly similar and the phase accumulated by light traveling through the particle is very small. Such condition applies to a large class of particles, which include biological, macromolecular, and other low-index contrast structures.[66–72] Approximate methods become necessary especially when dealing with complex structures where rigor-

ous theory or numerical techniques become impractical or too intensive. Two commonly used approximations are the Rayleigh-Gans-Debye (RGD) and Wentzel-Kramers-Brillouin (WKB) methods.[66–72] Within the RGD model, the internal field is assumed to be the same as the incident field. This model is roughly valid under two conditions: (1) $|m-1| \ll 1$, where m is the relative index between the particle and its environment, and (2) $4\pi R|m-1|/\lambda \ll 1$, where R is a characteristic dimension of the particle. For the WKB technique, the internal field is equal to the incident field modulated by a phase delay factor that corresponds to an additional phase shift experienced by the wave propagating inside the particle. Consequently, the WKB method serves as a refinement of the RGD model and has been shown to be relatively successful in predicting scattering patterns for nonspherical objects.[72]

Unlike the case of linear optical scattering, the lack of contrast in the dielectric functions of the particle and the surrounding medium does not imply a weak response for nonlinear optical scattering. Thus, the RGD model has a wide range of applicability to nonlinear scattering problems of practical interest. For example, several recent experiments from spherical particles possessing centrosymmetric media, which exhibit either low or no index contrast with their environment, e.g., liposomes, vesicles, cells, oil emulsions, or polystyrene in liquids, have demonstrated the intrinsic sensitivity of SHG to the particles' surfaces.[14,15] To describe the nonlinear optical response of low-index contrast particle systems, workers have employed the scattering approximations described above. The RGD model has been applied to the case of SHG and SFG scattering from a sphere of centrosymmetric medium[23,49,52–54,73,74] with excellent agreement with experiments.[52,73,74] The WKB method has been developed to describe SFG from a sphere that has a slight index mismatch with its environment.[53] Because of the inherent simplicity of the RGD model and its success in predicting the angular patterns of the SH radiation in spheres, we restrict ourselves to the RGD model in calculating the SH scattering from finite cylinders. The RGD model yields the SH field for a finite cylinder, which can be expressed in an analytical form, and reveals a myriad of novel features associated with this seemingly simple scattering process.

In applying the RGD model to describe SHG from a finite cylinder, we have considered both cases of particles comprised of noncentrosymmetric and centrosymmetric media. As presented in this paper, for noncentrosymmetric media we obtained the following results: (1) The nonlinear optical vector form factor may be expressed as a simple product of the linear optical form factor and the vector nonlinear susceptibility that is derived from a contraction of the nonlinear optical susceptibility tensor with the two fundamental field polarizations. Thus, a single scattering form factor governs the scattering process for all the nonlinear susceptibility elements. (2) For the forward scattering geometry, the nonlinear form factor is independent of the dimensions of the particle and depends only on the crystallographic orientation and the polarization of the fundamental field. (3) In the Rayleigh limit of a small cylinder, the SH field scales as $E^{(2\omega)} \sim a^2 L/\lambda^2$, where a and L are the radius and length of the cylinder, respectively, and λ is the fundamental wavelength. For the case of a cylinder possessing centrosymmetric medium, we obtain the following features: (1) In contrast to the noncentrosymmetric case, each surface nonlinear optical susceptibility element may experience multiple scattering form factors. (2) The *effective susceptibility* of the particle,[53] which can be thought of as a nonlinear optical polarizability of the particle, has 18 independent elements even if the local surface symmetry is isotropic without a mirror plane. In contrast, a sphere comprising centrosymmetric bulk medium of *arbitrary* surface symmetry has only four independent effective nonlinear susceptibility elements. (3) In the forward scattering direction, the nonlinear optical response of the cylinder corresponds to an effective C_∞ symmetry, so that the effective susceptibility has only four independent elements for a surface of arbitrary symmetry. These four elements arise from a linear combination of seven independent surface nonlinear susceptibility elements. The remaining 11 independent surface nonlinear susceptibility terms do not contribute to the forward scattering direction. (4) It is known that for randomly oriented chiral molecules, SHG is forbidden, but SFG is allowed. However, when these chiral molecules are adsorbed on a single cylindrical particle, SHG becomes allowed. An effective chiral axis may form along the cylindrical axis under several geometrical conditions, such as the forward scattering configuration or when $a \ll \lambda$. Under these conditions, the effective chiral susceptibility arises purely from the surface chiral sources. (5) In the Rayleigh limit, the SH field $E^{(2\omega)}$ may scale either as $\sim a^2 L/\lambda^3$ or $\sim aL/\lambda^2$. The latter scaling arises when at least one of the "forward emitting" surface susceptibility elements is present, such as the chiral susceptibility. With regards to the effect of the finite length of the cylinder, the SH signal is found to be an oscillatory function of the cylinder's length for both noncentrosymmetric and centrosymmetric cases.

The scope of this paper is as follows: In Sec. II, we develop the theory of SH scattering by calculating the nonlinear form factor and the effective nonlinear optical susceptibility of the particle for both noncentrosymmetric and centrosymmetric media. Section III is devoted to examples and discussion of some important features of SH scattering, such as the radiation pattern. In particular, we consider the bulk or the local surface symmetry belonging to the symmetry classes C_∞, C_6, and C_4. We then analyze the results for certain special geometries, such as forward scattering and limiting cases for Rayleigh-sized particles, wires, and disks, the chiral nonlinear response, and polarization dependence.

II. THEORETICAL DESCRIPTION

The starting point for the derivation of the SH field is the vector potential $\mathbf{A}(\mathbf{r})$. Within the Lorentz gauge, the vector potential $\mathbf{A}(\mathbf{r})$ for SHG arising from a current-density source $\mathbf{J}(\mathbf{r}')$ or nonlinear polarization $\mathbf{P}^{(2\omega)}(\mathbf{r}')$ is given by[75]

$$\mathbf{A}(\mathbf{r}) = \frac{1}{c}\int \frac{\exp(iK_1|\mathbf{r}-\mathbf{r}'|)\mathbf{J}(\mathbf{r}')}{|\mathbf{r}-\mathbf{r}'|}d\mathbf{r}' = \frac{K}{i}\int \frac{\exp(iK_1|\mathbf{r}-\mathbf{r}'|)\mathbf{P}^{(2\omega)}(\mathbf{r}')}{|\mathbf{r}-\mathbf{r}'|}d\mathbf{r}', \quad (1)$$

where $\mathbf{r}$ and $\mathbf{r}'$ denote the field and source points, respec-

tively, $K_1=n(2\omega)2\omega/c=n(2\omega)K$ is the magnitude of the scattered wave vector $\mathbf{K}_1$ $(=K_1\hat{\mathbf{r}})$; K is the magnitude of vacuum SH wave vector; and n is the refractive index of the medium. The second equality arises from the relation $\mathbf{J}(\mathbf{r}',t)=\partial\mathbf{P}^{(2\omega)}(\mathbf{r}',t)/\partial t$. The vector quantities $\mathbf{J}(\mathbf{r})$, $\mathbf{P}^{(2\omega)}(\mathbf{r})$, and $\mathbf{A}(\mathbf{r})$ represent complex spatial amplitudes for the physical quantities according to the relation $\mathbf{G}(\mathbf{r},t)=2\,\mathrm{Re}[\mathbf{G}(\mathbf{r})\exp(-im\omega t)]$, where $m=1$ or 2 corresponds to the fundamental or SH frequency. For simplicity, we assume plane-wave excitation. The analysis may be extended to the case of focused beam geometry, as considered theoretically for the case of spheres[51] and membranes.[76]

The nonlinear optical polarization may be expressed as[6]

$$\mathbf{P}^{(2\omega)}(\mathbf{r}')=\vec{\vec{\chi}}^{(2)}:\mathbf{E}^{(\omega)}(\mathbf{r}')\mathbf{E}^{(\omega)}(\mathbf{r}')+\vec{\vec{\chi}}_s^{(2)}:\mathbf{E}^{(\omega)}(\mathbf{r}')\mathbf{E}^{(\omega)}(\mathbf{r}')\times\delta[r'-h(r')]+\vec{\vec{\chi}}_b^{(2)}\vdots\mathbf{E}^{(\omega)}(\mathbf{r}')\nabla\mathbf{E}^{(\omega)}(\mathbf{r}'),\tag{2}$$

where $\mathbf{E}^{(\omega)}(\mathbf{r}')$ is the fundamental field at the source point $\mathbf{r}'$. From this point forward, we employ the RGD approximation in our calculations; in particular, the source field $\mathbf{E}^{(\omega)}(\mathbf{r}')$ is equated to the incident field, denoted by $\mathbf{E}_0^{(\omega)}(\mathbf{r})=\hat{\boldsymbol{\epsilon}}_0E_0\exp(i\mathbf{k}_1\cdot\mathbf{r})$, where $\mathbf{k}_1=k_1\hat{\mathbf{k}}$, $k_1=n(\omega)\omega/c=n(\omega)k$ is the magnitude of the fundamental wave vector $\mathbf{k}_1$, k is the magnitude of vacuum fundamental wave vector, and $\hat{\boldsymbol{\epsilon}}_0$ is the unit polarization vector of the input field. Thus, $\mathbf{E}^{(\omega)}(\mathbf{r}')=\mathbf{E}_0^{(\omega)}(\mathbf{r}')$. The local response of the medium is described by the bulk and surface nonlinear susceptibility tensors $\vec{\vec{\chi}}^{(2)}$ and $\vec{\vec{\chi}}_s^{(2)}$, respectively, while the leading-order nonlocal response is described by the nonlinear susceptibility $\vec{\vec{\chi}}_b^{(2)}$. The function $h(r')$ defines the boundary of the surface. Evaluating Eq. (2), we may write the nonlinear polarization as

$$\mathbf{P}^{(2\omega)}(\mathbf{r}')=E_0^2\boldsymbol{\chi}(\mathbf{r}')\exp(i2\mathbf{k}_1\cdot\mathbf{r}'),\tag{3}$$

where $\boldsymbol{\chi}(\mathbf{r}')$ is the nonlinear optical susceptibility vector defined as

$$\boldsymbol{\chi}(\mathbf{r}')=\vec{\vec{\chi}}^{(2)}:\hat{\boldsymbol{\epsilon}}_0\hat{\boldsymbol{\epsilon}}_0+\vec{\vec{\chi}}_s^{(2)}:\hat{\boldsymbol{\epsilon}}_0\hat{\boldsymbol{\epsilon}}_0\delta[r'-h(r')]+i\vec{\vec{\chi}}_b^{(2)}\vdots\hat{\boldsymbol{\epsilon}}_0\mathbf{k}_1\hat{\boldsymbol{\epsilon}}_0.\tag{4}$$

In the far-field zone, $r\gg r'$, where $r=|\mathbf{r}|$ and $r'=|\mathbf{r}'|$, the term $\exp(iK_1|\mathbf{r}-\mathbf{r}'|)\approx\exp[iK_1(r-\hat{\mathbf{r}}\cdot\mathbf{r}')]$ in the integral of Eq. (1). Substituting Eq. (3) into Eq. (1), we obtain

$$\mathbf{A}(\mathbf{r})=\frac{K\exp(iK_1r)VE_0^2\mathbf{p}}{ir},\tag{5}$$

where V is the volume of the particle and $\mathbf{p}$ is the vector nonlinear susceptibility form factor or, simply, the nonlinear form factor, which is proportional to the effective dipole moment, and is given by

$$\mathbf{p}=\frac{1}{V}\int_V\boldsymbol{\chi}(\mathbf{r}')\exp(i\mathbf{q}\cdot\mathbf{r}')d\mathbf{r}',\tag{6}$$

and $\mathbf{q}\equiv2\mathbf{k}_1-\mathbf{K}_1$ is the wave-vector transfer. The SH field is obtained using the relation $\mathbf{E}^{(2\omega)}(\mathbf{r})=iK[\hat{\mathbf{r}}\times\mathbf{A}(\mathbf{r})]\times\hat{\mathbf{r}}$, where $\mathbf{A}(\mathbf{r})$ is given by Eq. (5), which yields

$$\mathbf{E}^{(2\omega)}=\frac{K^2\exp(iK_1r)VE_0^2}{r}(\hat{\mathbf{r}}\times\mathbf{p})\times\hat{\mathbf{r}}.\tag{7}$$

A. Small index difference

Before embarking on the investigation of SH scattering using the RGD model, we take a brief digression by considering the WKB method for the case of small refractive-index difference between the particle and its environment. Within the WKB approximation, the incident beam is assumed to be undeflected by the particle but is allowed to acquire phase in proportion to the degree of penetration into the particle as the fundamental field propagates from an entrance position $\mathbf{r}_1'$ into an interior position $\mathbf{r}'$ of the particle. Likewise, one may also stipulate that the SH wave propagate rectilinearly and experience a local phase delay as it propagates from the generation point $\mathbf{r}'$ to some point $\mathbf{r}_2'$ just outside the particle. Thus, the phase term given by $\mathbf{q}\cdot\mathbf{r}'$ in Eq. (6) may be replaced by $\mathbf{q}\cdot\mathbf{r}'+2\Delta\mathbf{k}_1\cdot(\mathbf{r}'-\mathbf{r}_1')-\Delta\mathbf{K}_1\cdot(\mathbf{r}'-\mathbf{r}_2')$, where the second term is twice the excess phase delay experienced locally by the fundamental wave, and the third term corresponds to the excess phase delay experienced by the SH wave as it exits the particle. The quantities $\Delta\mathbf{k}_1$ and $\Delta\mathbf{K}_1$ are given by $\Delta\mathbf{k}_1=\Delta n_\omega\,k\,\hat{\mathbf{k}}$ and $\Delta\mathbf{K}_1=\Delta n_{2\omega}K\,\hat{\mathbf{r}}$, where $\Delta n_{m\omega}=n_{\mathrm{in}}(m\omega)-n_{\mathrm{out}}(m\omega)$ is the difference between the refractive indices of the particle and the environment at angular frequency $m\omega$, with $m=1$ or 2. The phase factor may be written as $\phi=\mathbf{q}'\cdot\mathbf{r}'+[(2\Delta\mathbf{k}_1-\Delta\mathbf{K}_1)\cdot(\mathbf{r}_2'-\mathbf{r}_1')]$, where $\mathbf{q}'=2(\mathbf{k}_1+\Delta\mathbf{k}_1)-(\mathbf{K}_1+\Delta\mathbf{K}_1)$. Note that in the absence of the second term in ϕ, which is proportional to $(\Delta n_\omega\hat{\mathbf{k}}-\Delta n_{2\omega}\hat{\mathbf{r}})\cdot(\mathbf{r}_2'-\mathbf{r}_1')$, the problem is mathematically identical to the RGD model with $\mathbf{q}$ replaced by $\mathbf{q}'$. The presence of this second term, however, may significantly complicate the integration in Eq. (6) and lead to a nonanalytical expression for the SH field. Hence, in this paper, we have limited our investigation to the case of the RGD model that is sufficient in describing the zeroth-order behavior of the nonlinear optical response of a finite cylindrical particle. It should be noted that other workers have considered nonindex-matched structures, e.g., infinite two-dimensional structures[58] or thin wires[5,60] but with the restriction of the fundamental wave traveling parallel or orthogonal to the axis, and for specific material symmetry.

B. Scattering geometry and parameters

Figure 1 illustrates the scattering geometry. The scattering plane is defined by the directions of the incident fundamental and the scattered SH waves, which are specified by the fundamental and SH wave vectors $\mathbf{k}_1=k_1\hat{\mathbf{z}}$ and $\mathbf{K}_1=K_1\hat{\mathbf{r}}$, respectively, where $\hat{\mathbf{r}}=(\sin\theta\cos\varphi\hat{\mathbf{x}}+\sin\theta\sin\varphi\hat{\mathbf{y}}+\cos\theta\hat{\mathbf{z}})$. The particle is fixed with respect to the coordinates $(\hat{\mathbf{x}}',\hat{\mathbf{y}}',\hat{\mathbf{z}}')$ with the cylindrical axis parallel to $\hat{\mathbf{z}}'$; this particle frame is arbitrarily oriented relative to the laboratory frame $(\hat{\mathbf{x}},\hat{\mathbf{y}},\hat{\mathbf{z}})$. We interchangeably denote the laboratory axes (x,y,z) by (x_1,x_2,x_3), the particle reference axes (x',y',z') by (x_1',x_2',x_3'), and the crystallographic axes (x'',y'',z'') by (x_1'',x_2'',x_3''). We assume the following transformations between these coordinate frames:

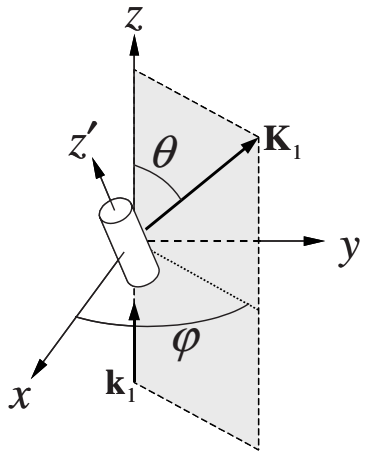

FIG. 1. Geometry of second-harmonic scattering from a finite cylinder.

$$x_i' = M_{ij}' x_j, \tag{8a}$$

$$x_i'' = M_{ij}'' x_j', \tag{8b}$$

where M_{ij}' (M_{ij}'') is an element of the transformation matrix $\mathbf{M}'$ ($\mathbf{M}''$) between the particle (crystallographic) and laboratory (particle) frames of reference.

Throughout this paper, we have adopted the Einstein summation convention for terms with repeated indices unless noted otherwise. We assume that the laboratory and particle reference frames are related through an Euler transformation that employs the sequence of rotations in Fig. 2 to define the Euler transformation matrix

$$\mathbf{M}(\alpha,\beta,\varsigma) = R_z(\varsigma)R_y(\beta)R_z(\alpha), \tag{9}$$

where $R_i(\alpha)$ is the rotation matrix obtained through a (counterclockwise) rotation of α about the x_i axis. We then obtain the relation $x_i' = M_{ij}(\alpha,\beta,\varsigma)x_j$. Because of the axial symmetry of the cylinder, the choice of ς is immaterial so we may set $\varsigma=0$. For the noncentrosymmetric case, we assume a rotation matrix of $\mathbf{M}(\xi,\eta,\zeta)$ linking the crystallographic and particle reference frames, $x_i'' = M_{ij}(\xi,\eta,\zeta)x_j'$. Using Eqs. (8a), (8b), and (9), we obtain

$$M_{ij}' \equiv M_{ij}(\alpha,\beta,0), \tag{10a}$$

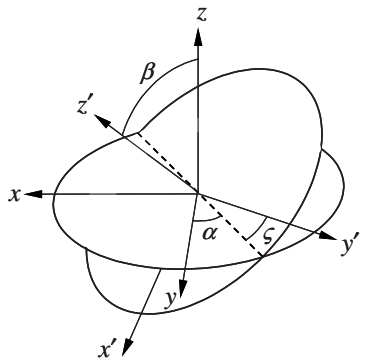

FIG. 2. Euler transformation for a sequence of rotations described by the transformations $R_z(\alpha)$, $R_y(\beta)$, and $R_z(\varsigma)$.

$$M_{ij}'' \equiv M_{ij}(\xi,\eta,\zeta). \tag{10b}$$

The source vector $\mathbf{r}'$, which is expressed in terms of the particle basis vectors, may be written in Cartesian (x',y',z') or cylindrical coordinates (ρ',φ',z') as

$$\mathbf{r}' = x'\hat{\mathbf{x}}' + y'\hat{\mathbf{y}}' + z'\hat{\mathbf{z}}' = \rho'\hat{\boldsymbol{\rho}}' + z'\hat{\mathbf{z}}'. \tag{11}$$

The cylindrical coordinate system provides a natural set of coordinates for the source points located at the curved side of the cylinder. In particular, the unit vectors $\hat{\boldsymbol{\rho}}' = \cos\varphi'\,\hat{\mathbf{x}}' + \sin\varphi'\hat{\mathbf{y}}'$, $\hat{\boldsymbol{\varphi}}' = -\sin\varphi'\hat{\mathbf{x}}' + \cos\varphi'\hat{\mathbf{y}}'$, and $\hat{\mathbf{z}}'$ will be used in describing the input electric field vector and the nonlinear polarization at the curved portion of the cylinder. For an input radiation propagating along the $\hat{\mathbf{z}}$ direction, its unit polarization vector may be expressed in the laboratory or particle coordinates as

$$\hat{\boldsymbol{\epsilon}}_0 = \epsilon_{01}\hat{\mathbf{x}} + \epsilon_{02}\hat{\mathbf{y}} = \mathcal{E}_1\hat{\mathbf{x}}' + \mathcal{E}_2\hat{\mathbf{y}}' + \mathcal{E}_3\hat{\mathbf{z}}' = \mathcal{E}_{\rho'}\hat{\boldsymbol{\rho}}' + \mathcal{E}_{\varphi'}\hat{\boldsymbol{\varphi}}' + \mathcal{E}_3\hat{\mathbf{z}}', \tag{12}$$

where the component $\mathcal{E}_i$ in the particle frame is related to the component ϵ_{0j} in the laboratory frame through $\mathcal{E}_i = M_{ij}'\epsilon_{0j}$; in cylindrical coordinates, its components are given by $\mathcal{E}_{\rho'} = (\mathcal{E}_1\cos\varphi' + \mathcal{E}_2\sin\varphi')$ and $\mathcal{E}_{\varphi'} = (\mathcal{E}_2\cos\varphi' - \mathcal{E}_1\sin\varphi')$.

One important parameter is the phase term $\mathbf{q}\cdot\mathbf{r}'$ that is used in Eq. (6). We assume that the medium is dispersionless, i.e., $|2\mathbf{k}_1| = |\mathbf{K}_1| = K_1$, so that

$$\mathbf{q} = K_1(\hat{\mathbf{z}} - \hat{\mathbf{r}}), \tag{13}$$

whose magnitude is given by $q = |\mathbf{q}| = 2K_1\sin(\theta/2)$. The wave-vector transfer $\mathbf{q}$ can be expressed in the laboratory and particle frames as

$$\mathbf{q} = q_1\hat{\mathbf{x}} + q_2\hat{\mathbf{y}} + q_3\hat{\mathbf{z}} = Q_1\hat{\mathbf{x}}' + Q_2\hat{\mathbf{y}}' + Q_3\hat{\mathbf{y}}', \tag{14}$$

where $q_1 = -K_1\sin\theta\cos\varphi$, $q_2 = -K_1\sin\theta\sin\varphi$, $q_3 = K_1(1-\cos\theta)$, and $Q_i = M_{ij}'q_j$. Thus, using Eqs. (11) and (14), we obtain

$$\mathbf{q}\cdot\mathbf{r}' = Q_1\rho'\cos\varphi' + Q_2\rho'\sin\varphi' + Q_3z'. \tag{15}$$

C. Noncentrosymmetric media

We now consider the case of a particle possessing single-domain, noncentrosymmetric medium. We may further assume that it has an arbitrary shape. For a noncentrosymmetric medium, the second and third terms in Eq. (4) are extremely weak compared to the first term and, thus, are neglected in this calculation. The leading term $\vec{\boldsymbol{\chi}}^{(2)}:\hat{\boldsymbol{\epsilon}}_0\hat{\boldsymbol{\epsilon}}_0$ in Eq. (4), which is a contraction of the nonlinear susceptibility tensor with the two fundamental unit polarization vectors, is a constant vector that is independent of the source vector $\mathbf{r}'$; hence, this term can be taken out of the integral of Eq. (6) to yield

$$\mathbf{p} = f\,\boldsymbol{\chi}_0, \tag{16}$$

where

$$f = \frac{1}{V}\int_V \exp(i\mathbf{q}\cdot\mathbf{r}')d\mathbf{r}' \tag{17}$$

and

$$\boldsymbol{\chi}_0 = \vec{\boldsymbol{\chi}}^{(2)}:\hat{\boldsymbol{\epsilon}}_0\hat{\boldsymbol{\epsilon}}_0. \tag{18}$$

The function f is the usual form factor commonly known in linear optical scattering, which has the property $f=1$ for the case of forward scattering ($\mathbf{q}=0$). Thus, Eq. (16) shows that the nonlinear form factor $\mathbf{p}$ of a bulk nonlinear active particle can be described as a simple product of the linear optical form factor f and the susceptibility vector $\boldsymbol{\chi}_0$. This property implies that all the nonlinear tensor elements experience the same scattering form factor f. Furthermore, Eq. (16) is valid for an arbitrarily shaped particle satisfying the RGD conditions and for a noncentrosymmetric medium of arbitrary symmetry.

The form factor for a cylinder of radius a and length L, with the flat sides defined by $z'=\pm L/2$, is given by[67,68]

$$f = 2\frac{\sin(Q_3\Lambda a)}{Q_3\Lambda a}\frac{J_1(Qa)}{Qa}, \tag{19}$$

where $\Lambda=L/2a$ is the aspect ratio, $Q_3=\mathbf{q}\cdot\hat{\mathbf{z}}'$, and Q is the magnitude of the component of $\mathbf{q}$ perpendicular to $\mathbf{z}'$, i.e.,

$$Q = (Q_1^2 + Q_2^2)^{1/2} \tag{20}$$

and J_n is the Bessel function of the first kind of order n. The vector $\boldsymbol{\chi}_0$ may be written in terms of the crystallographic unit basis vectors or the particle coordinates, i.e., $\boldsymbol{\chi}_0=\chi''_{0i}\hat{\mathbf{x}}''_i=\chi'_{0i}\hat{\mathbf{x}}'_i$, to yield

$$\chi''_{0i} = \chi^{(2)}_{ijk}(\hat{\boldsymbol{\epsilon}}_0\cdot\hat{\mathbf{x}}''_j)(\hat{\boldsymbol{\epsilon}}_0\cdot\hat{\mathbf{x}}''_k), \tag{21a}$$

$$\chi'_{0l} = \chi^{(2)}_{ijk}M''_{il}M''_{jm}M''_{kn}\mathcal{E}_m\mathcal{E}_n, \tag{21b}$$

where the nonlinear susceptibility element $\chi^{(2)}_{ijk}$ is expressed in the crystallographic reference frame. In obtaining Eq. (21b), we made use of Eqs. (8b) and (12). By means of Eqs. (17) and (21b), the nonlinear form factor $\mathbf{p}$ may be written in terms of the particle coordinates, i.e., $\mathbf{p}=p'_i\hat{\mathbf{x}}'_i$, where

$$p'_i = \chi^{\text{eff}}_{ijk}\mathcal{E}_j\mathcal{E}_k \tag{22}$$

and

$$\chi^{\text{eff}}_{ijk} = f\chi'^{(2)}_{ijk} = f\chi^{(2)}_{lmn}M''_{li}M''_{mj}M''_{nk} \tag{23}$$

is the effective susceptibility in the particle frame. The concept of the effective susceptibility was introduced in Ref. 53 to describe the effective nonlinear polarizability of a particle in the principal (i.e., the particle) reference frame. This useful quantity is dependent not only on the material susceptibilities but also on the particle's dimensions and the difference between the scattered and input wave vectors. It should be noted that χ^{eff}_{ijk} is equivalent to the definition used in Refs. 53 and 54 except for a minor difference in the normalization constant arising from the $1/V$ factor in Eq. (16). Equation (22) is a general expression that is valid even for the case of centrosymmetric medium, as will be shown in Sec. II D.

Before we proceed with the case of the particle comprised of centrosymmetric medium, we make a few remarks regarding the general formula given by Eq. (16) on the dependence of $\mathbf{p}$ on various material, geometrical, and optical parameters. We begin by examining its two constituent factors: the form factor f and the nonlinear susceptibility vector $\boldsymbol{\chi}_0$. Inspecting Eqs. (15) and (17), we find that f depends on the particle dimensions, particle orientation, and the scattering angles. Examining Eq. (21b), we observe that $\boldsymbol{\chi}_0$ is independent of the particle dimensions but is dependent on the nonlinear susceptibility elements, the crystallographic orientation, and input-polarization state $\hat{\boldsymbol{\epsilon}}_0$. By exploring the polarization response of the SH scattering from the particle, one may, in principle, infer the orientation of the crystallographic axes. Recent studies have experimentally demonstrated the relationship between the crystallographic orientation in nanocrystals and the polarization properties of SHG.[2–5]

D. Centrosymmetric media

We now consider the case of a finite cylinder comprised of isotropic and centrosymmetric bulk medium. The first term in Eq. (4) vanishes so that we can write $\boldsymbol{\chi}=\boldsymbol{\chi}_s+\boldsymbol{\chi}_b$, where $\boldsymbol{\chi}_s$ and $\boldsymbol{\chi}_b$ are equal to the second and third terms of Eq. (4), respectively. The corresponding nonlinear form factor then arises from the surface contribution and a nonlocal bulk polarization source, which we denote by $\mathbf{p}_s$ and $\mathbf{p}_b$, respectively, i.e.,

$$\mathbf{p} = \mathbf{p}_s + \mathbf{p}_b = \mathbf{p}_s^{\text{flat}} + \mathbf{p}_s^{\text{curved}} + \mathbf{p}_b. \tag{24}$$

The terms $\mathbf{p}_s^{\text{flat}}$ and $\mathbf{p}_s^{\text{curved}}$ are contributions originating from the flat circular caps and the curved wall of the cylinder, respectively. Let us first consider the vector $\mathbf{p}_b$ because it is simpler to evaluate. Its corresponding $\boldsymbol{\chi}(\mathbf{r}')$ term in Eq. (4) reduces to a simple expression $\boldsymbol{\chi}_b=2i\gamma(\hat{\boldsymbol{\epsilon}}_0\cdot\hat{\boldsymbol{\epsilon}}_0)\mathbf{k}_1$, where $\gamma=\chi^{(2)}_{b,\ ijij}/2$. Here, $\chi^{(2)}_{b,\ ijij}=\chi^{(2)}_{b,\ 1212}$ (not summed) is one of the independent tensor elements of $\vec{\boldsymbol{\chi}}^{(2)}_b$. Noting that $\boldsymbol{\chi}_b$ is a constant vector, we obtain, as in the case of the derivation leading to Eq. (16), $\mathbf{p}_b=i\gamma(\hat{\boldsymbol{\epsilon}}_0\cdot\hat{\boldsymbol{\epsilon}}_0)f\,K_1\hat{\mathbf{z}}$ where f is given by Eq. (19). Furthermore, if we add to $\mathbf{p}_b$ a term that is proportional to $\hat{\mathbf{r}}$, the resulting SH field due to $\mathbf{p}_b$ is not altered as can be seen from Eq. (7). Thus, we may write $\mathbf{p}_b=i\gamma(\hat{\boldsymbol{\epsilon}}_0\cdot\hat{\boldsymbol{\epsilon}}_0)f\,K_1(\hat{\mathbf{z}}-\hat{\mathbf{r}})$ or

$$\mathbf{p}_b = i\gamma(\hat{\boldsymbol{\epsilon}}_0\cdot\hat{\boldsymbol{\epsilon}}_0)f\mathbf{q} \tag{25}$$

using Eq. (13).

The surface contribution $\mathbf{p}_s$ is given by

$$\mathbf{p}_s = \frac{1}{V}\int_V \vec{\boldsymbol{\chi}}^{(2)}_s:\hat{\boldsymbol{\epsilon}}_0\hat{\boldsymbol{\epsilon}}_0\delta[r'-h(r')]\exp(i\mathbf{q}\cdot\mathbf{r}')\,d\mathbf{r}'. \tag{26}$$

Integrating with respect to r' reduces the volume integral in Eq. (26) into a surface integral that consists of three regions: the two "top" and "bottom" flat sides, which correspond to the terms $\delta(z-L/2)$ and $\delta(z+L/2)$, respectively, and the curved surface of the cylinder, which corresponds to the term $\delta(\rho'-a)$. For the flat sides ($z'=\pm L/2$), the vector $\vec{\boldsymbol{\chi}}^{(2)}_s:\hat{\boldsymbol{\epsilon}}_0\hat{\boldsymbol{\epsilon}}_0=\hat{\mathbf{x}}'_i\chi^{(2)}_{s,\ ijk}\mathcal{E}_j\mathcal{E}_k$ (in terms of the particle coordinates) is constant and, thus, may be taken out of the integral in Eq. (26). Integrating Eq. (26) over the surfaces corresponding to

$z' = \pm L/2$ and combining the two terms, we obtain

$$\mathbf{p}_s^{\text{flat}} = iQ_3 \vec{\boldsymbol{\chi}}_s^{(2)} : \hat{\boldsymbol{\epsilon}}_0 \hat{\boldsymbol{\epsilon}}_0 f. \tag{27}$$

The vector $\mathbf{p}_s^{\text{curved}}$ arises from the curved part of the cylinder corresponding to $\rho' = a$. For this surface, the term $\vec{\boldsymbol{\chi}}_s^{(2)} : \hat{\boldsymbol{\epsilon}}_0 \hat{\boldsymbol{\epsilon}}_0$ is a vector whose direction depends on the location of the source vector $\boldsymbol{\rho}' = a\hat{\boldsymbol{\rho}}'$, i.e., it depends on the azimuthal angle φ' and, hence, cannot be taken out of the integral in Eq. (26). Details of this calculation are presented in Appendix A. For any tensor element $\chi_{s,ijk}^{(2)}$, direct integration of Eq. (26) over the curved portion of the particle yields

$$\mathbf{p}_s^{\text{curved}} = \frac{1}{\pi a} \frac{\sin(Q_3 \Lambda a)}{Q_3 \Lambda a} \boldsymbol{\Gamma}, \tag{28}$$

where $\boldsymbol{\Gamma} = \int_0^{2\pi} \vec{\boldsymbol{\chi}}_s^{(2)} : \hat{\boldsymbol{\epsilon}}_0 \hat{\boldsymbol{\epsilon}}_0 \exp(ia\, \mathbf{q} \cdot \hat{\boldsymbol{\rho}}') d\varphi' = \int_0^{2\pi} \vec{\boldsymbol{\chi}}_s^{(2)} : \hat{\boldsymbol{\epsilon}}_0 \hat{\boldsymbol{\epsilon}}_0 \exp[ia(Q_1 \cos\varphi' + Q_2 \sin\varphi')] d\varphi'$. In terms of the particle frame, $\boldsymbol{\Gamma} = \Gamma_i' \hat{\mathbf{x}}_i'$ where

$$\begin{aligned}\Gamma_i' = \chi_{s,\ \alpha\beta\gamma}^{(2)} \{ & I_3(\delta_{i1}\delta_{\alpha\rho'} + \delta_{i2}\delta_{\alpha\varphi'}, \delta_{i2}\delta_{\alpha\rho'} - \delta_{i1}\delta_{\alpha\varphi'}; \mathcal{E}_1\delta_{\beta\rho'} + \mathcal{E}_2\delta_{\beta\varphi'}, \mathcal{E}_2\delta_{\beta\rho'} - \mathcal{E}_1\delta_{\beta\varphi'}; \mathcal{E}_1\delta_{\gamma\rho'} + \mathcal{E}_2\delta_{\gamma\varphi'}, \mathcal{E}_2\delta_{\gamma\rho'} - \mathcal{E}_1\delta_{\gamma\varphi'}) \\ & + [I_2(\delta_{i1}\delta_{\alpha\rho'} + \delta_{i2}\delta_{\alpha\varphi'}, \delta_{i2}\delta_{\alpha\rho'} - \delta_{i1}\delta_{\alpha\varphi'}; \mathcal{E}_1\delta_{\beta\rho'} + \mathcal{E}_2\delta_{\beta\varphi'}, \mathcal{E}_2\delta_{\beta\rho'} - \mathcal{E}_1\delta_{\beta\varphi'})\mathcal{E}_3\delta_{\gamma z'} + (\beta \leftrightarrow \gamma)] + I_1(\delta_{i1}\delta_{\alpha\rho'} + \delta_{i2}\delta_{\alpha\varphi'}, \delta_{i2}\delta_{\alpha\rho'} \\ & - \delta_{i1}\delta_{\alpha\varphi'})\mathcal{E}_3^2\delta_{\beta z'}\delta_{\gamma z'}\} + \delta_{i3}\chi_{s,\ z'\beta\gamma}^{(2)} \{ I_2(\mathcal{E}_1\delta_{\beta\rho'} + \mathcal{E}_2\delta_{\beta\varphi'}, \mathcal{E}_2\delta_{\beta\rho'} - \mathcal{E}_1\delta_{\beta\varphi'}; \mathcal{E}_1\delta_{\gamma\rho'} + \mathcal{E}_2\delta_{\gamma\varphi'}, \mathcal{E}_2\delta_{\gamma\rho'} - \mathcal{E}_1\delta_{\gamma\varphi'}) + [I_1(\mathcal{E}_1\delta_{\beta\rho'} \\ & + \mathcal{E}_2\delta_{\beta\varphi'}, \mathcal{E}_2\delta_{\beta\rho'} - \mathcal{E}_1\delta_{\beta\varphi'})\mathcal{E}_3\delta_{\gamma z'} + (\beta \leftrightarrow \gamma)] + I_0\mathcal{E}_3^2\delta_{\beta z'}\delta_{\gamma z'}\}\end{aligned} \tag{29}$$

and each index α, β, or γ refers to the local coordinate ρ', φ', or z'. The expression $(\beta \leftrightarrow \gamma)$ denotes the immediately preceding expression with indices β and γ interchanged. The terms I_0, I_1, I_2, and I_3 are integrals defined in Appendix A and are evaluated to be

$$I_0 = 2\pi J_0(\delta_0), \tag{30a}$$

$$I_1(A,B) = 2\pi i J_1(\delta_0)(A \cos\mu + B \sin\mu), \tag{30b}$$

$$\begin{aligned}I_2(A_1,B_1;A_2,B_2) = 2\pi \Big\{ & -J_2(\delta_0) \prod_{j=1}^{2} (A_j \cos\mu + B_j \sin\mu) \\ & + [J_1(\delta_0)/\delta_0](A_1A_2 + B_1B_2) \Big\},\end{aligned} \tag{30c}$$

$$\begin{aligned}I_3(A_1,B_1;A_2,B_2;A_3,B_3) = & \ 2\pi i \Big\{ -J_3(\delta_0) \prod_{j=1}^{3} (A_j \cos\mu + B_j \sin\mu) + [J_2(\delta_0)/\delta_0] \\ & \times [(3A_1A_2A_3 + A_1B_2B_3 + A_2B_1B_3 + A_3B_1B_2)\cos\mu \\ & + (3B_1B_2B_3 + B_1A_2A_3 + B_2A_1A_3 + B_3A_1A_2)\sin\mu] \Big\},\end{aligned} \tag{30d}$$

where $\delta_0 = Qa$, $\cos\mu = Q_1/Q$, and $\sin\mu = Q_2/Q$. Note that the Bessel functions in Eqs. (30a)–(30d) may be transformed into Bessel functions of other orders by using the identity $J_{n-1}(\delta_0) + J_{n+1}(\delta_0) = 2nJ_n(\delta_0)/\delta_0$.

The nonlinear form factor for a cylinder possessing centrosymmetric medium, given by Eq. (24), holds true for a general surface nonlinear response. With the aid of Eqs. (29) and (30a)–(30d), $\mathbf{p}$ is obtained by expanding Eqs. (25), (27), and (28). Inspecting these equations, we note that each component p_i' of $\mathbf{p}$ in the particle frame is expressed in terms of linear combinations of the product $\mathcal{E}_j\mathcal{E}_k$. Consequently, p_j' may also be described, as in the case of noncentrosymmetric medium, in terms of the effective nonlinear susceptibility tensor element χ_{ijk}^{eff} as $p_i' = \chi_{ijk}^{\text{eff}} \mathcal{E}_j \mathcal{E}_k$. Explicit expressions for χ_{ijk}^{eff} are presented in Sec. III B for the case of a general isotropic surface lacking mirror symmetry.

E. Calculation of the SH field and radiated power

The nonlinear form factor component p_i of $\mathbf{p} = p_i\hat{\mathbf{x}}_i$ in the laboratory frame may be obtained from the component p_j' in the particle frame according to the relation

$$p_i = M_{ij}'^T p_j', \tag{31}$$

where $M_{ij}'^T = M_{ji}'$ is an element of the transpose of matrix $\mathbf{M}'$. The SH field $\mathbf{E}^{(2\omega)}$ is then obtained according to Eq. (7). For the case of the cylinder, $\mathbf{M}'$ is defined according to Eq. (9). In this paper, we have also considered the case of the sphere, which requires a different definition for $\mathbf{M}'$. Because of the lack of a structural axis for a sphere, a natural and convenient particle reference frame would be based on the direction of the wave-vector transfer $\mathbf{q}$. The sphere problem is discussed in detail in Appendix B for SHG (and in Refs. 52–54 for SFG). The radiated SH power per unit solid angle may then be calculated using the equation $\mathcal{P}_\Omega \equiv d\mathcal{P}/d\Omega = [cr^2 n(2\omega)/(2\pi)]|\hat{\boldsymbol{\epsilon}}^* \cdot \mathbf{E}^{(2\omega)}(\mathbf{r})|^2$ for detection through an analyzer that passes polarization state $\hat{\boldsymbol{\epsilon}}$. Another important quantity that one may wish to compute, but is not considered in this paper, is the orientationally averaged power per unit solid angle given by $\langle \mathcal{P}_\Omega \rangle = (1/4\pi) \int_0^{2\pi} \int_0^{\pi} (d\mathcal{P}/d\Omega) \sin\beta d\beta d\alpha$, where α and β are the particle orientation angles defined in Eq. (10a). The quantity $\langle \mathcal{P}_\Omega \rangle$ may be used in describing, for example, the SH radiation patterns of a collection of randomly oriented monodisperse cylinders in a solution.

III. SPECIAL CASES AND DISCUSSION

In the preceding section, we have calculated the SH nonlinear form factor $\mathbf{p}$, as well as the SH effective nonlinear

susceptibility tensor χ_{ijk}^{eff}, for a cylinder comprising noncentrosymmetric [through Eq. (23)] or centrosymmetric medium [through Eqs. (25) and (27)–(29)] of arbitrary symmetry. We now apply these results to specific bulk and surface symmetry classes.

A. Noncentrosymmetric case: Bulk symmetry classes C_∞, C_6, and C_4

1. Nonlinear form factor

For illustration purposes, we consider a particle whose medium possesses a symmetry that belongs to any of the following point group symmetry classes: C_∞, C_6, or C_4. For these symmetry classes, there are four independent nonlinear susceptibility elements for the SHG process given by $\chi_{z''z''z''}^{(2)}$, $\chi_{z''x''x''}^{(2)}=\chi_{z''y''y''}^{(2)}$, $\chi_{x''z''x''}^{(2)}=\chi_{y''z''y''}^{(2)}$, $\chi_{x''y''z''}^{(2)}=-\chi_{y''x''z''}^{(2)}$, which are expressed in terms of the crystallographic frame. If $s_i=\delta_{iz''}$ denotes the crystallographic symmetry axis, the nonlinear susceptibility tensor element $\chi_{ijk}^{(2)}$ may be expressed succinctly as

$$\chi_{ijk}^{(2)}=a''s_is_js_k+b''s_i\delta_{jk}+\frac{c''}{2}(s_j\delta_{ik}+s_k\delta_{ij})+\frac{d''}{2}(\varepsilon_{ijl}s_ls_k+\varepsilon_{ikl}s_ls_j), \tag{32}$$

where $\chi_{z''z''z''}^{(2)}=a''+b''+c''$, $\chi_{z''x''x''}^{(2)}=b''$, $\chi_{x''z''x''}^{(2)}=c''/2$, $\chi_{x''y''z''}^{(2)}=d''/2$, and ε_{ijk} is the Levi-Civita tensor. The first three elements provide the achiral response of the particle while the last element yields the chiral response. The form of the expression in Eq. (32) is similar to that previously derived in Ref. 77 except for the presence of the chiral term $\chi_{x''y''z''}^{(2)}$. Note that if Kleinman symmetry[78] is valid, $\chi_{z''x''x''}^{(2)}=\chi_{x''z''x''}^{(2)}$ and $\chi_{x''y''z''}^{(2)}=0$. In general, the crystallographic axes (x_i'') of the medium are arbitrarily oriented with respect to the particle frame according to Eq. (8b) so that $\chi_{ijk}'^{(2)}=\chi_{lmn}^{(2)}M_{li}''M_{mj}''M_{nk}''$, where $\chi_{ijk}'^{(2)}$ is the susceptibility in the particle frame. If the crystallographic and particle axes are aligned with each other, i.e., $M_{ij}''=\delta_{ij}$, then $\chi_{ijk}'^{(2)}=\chi_{ijk}^{(2)}$. Consequently, Eqs. (22), (23), and (32) yield

$$\mathbf{p}=f[a''\hat{\mathbf{s}}(\hat{\mathbf{s}}\cdot\hat{\boldsymbol{\epsilon}}_0)^2+b''\hat{\mathbf{s}}(\hat{\boldsymbol{\epsilon}}_0\cdot\hat{\boldsymbol{\epsilon}}_0)+c''\hat{\boldsymbol{\epsilon}}_0(\hat{\mathbf{s}}\cdot\hat{\boldsymbol{\epsilon}}_0)+d''(\hat{\mathbf{s}}\cdot\hat{\boldsymbol{\epsilon}}_0)(\hat{\boldsymbol{\epsilon}}_0\times\hat{\mathbf{s}})]. \tag{33}$$

The form factor f provides the SHG dependence on the particle orientation and scattering-angle direction. For an object of arbitrary size, f is maximized in the forward direction. The term inside the bracket also provides information about the dependence of the SHG signal on the particle orientation through $\hat{\mathbf{s}}$ and, in addition, on the input polarization. Making use of the vector properties of $\mathbf{p}$, one may be able to deduce all four independent nonlinear coefficients by applying, for example, an appropriate input-polarization geometry that selectively isolates or suppresses terms corresponding to the four susceptibility elements in Eq. (33). By examination of Eq. (33), a configuration with $\hat{\boldsymbol{\epsilon}}_0\perp\hat{\mathbf{s}}$ may be employed to obtain b'', whereas a configuration with $\hat{\boldsymbol{\epsilon}}_0\parallel\hat{\mathbf{s}}$ may be used to obtain an expression that relates the coefficients a'', b'', and c''. Circular polarization may be adopted to suppress the b'' term since $\hat{\boldsymbol{\epsilon}}_0\cdot\hat{\boldsymbol{\epsilon}}_0=0$. By noting further that $\mathbf{p}$ is proportional to the effective dipole moment and realizing that no radiation is emitted along its direction, one may collect data along the direction $\hat{\mathbf{s}}$, $\hat{\boldsymbol{\epsilon}}_0$, or $\hat{\boldsymbol{\epsilon}}_0\times\hat{\mathbf{s}}$, which suppresses the nonlinear response corresponding to a'' and b'', c'', or d'', respectively, according to Eq. (33).

A scheme in SH microscopy of fibrous structures, e.g., fibrillar collagen, typically makes use of a configuration where the cylindrical axis is set perpendicular to the beam direction, and the radiated SH signal detected along the forward or backward direction. Such a geometrical setup is a special case of the last configuration described above, i.e., observation along the $\hat{\boldsymbol{\epsilon}}_0\times\hat{\mathbf{s}}$ direction.[56,77,79–85] For this geometrical arrangement, the chiral contribution to the SH signal vanishes since $\hat{\boldsymbol{\epsilon}}_0\times\hat{\mathbf{s}}$ lies along $\hat{\mathbf{z}}$. However, we also see from Eq. (33) that provided $\hat{\boldsymbol{\epsilon}}_0$ and $\hat{\mathbf{s}}$ are not perpendicular or parallel, this chiral term may contribute to the total signal at observation points slightly away from the z direction. Hence, depending on the magnitude of $\chi_{x''y''z''}^{(2)}=d''/2$, the contribution from this term may become appreciable when using large numerical aperture lenses for collecting the SH signal. Moreover in the forward direction, for a fixed input polarization and arbitrary particle angle α, it can be shown by means of Eq. (33) that the maximum signal due to the chiral contribution occurs when $\beta=\pi/4$. For the general case of the crystallographic z'' axis aligned arbitrarily relative to the particle axis, one needs to make use of the more general expression given by Eq. (23) in calculating the nonlinear form factor.

2. Radiation patterns: Examples

We now consider an example in calculating the SH radiation patterns from a cylindrical object. We use the following parameters: $K_1a=1$ and $\Lambda=3$. These values may correspond to the following optical and geometrical parameters: $n=1.5$, $\lambda=800$ nm, $2a\approx 85$nm, and $L\approx 255$ nm. For the nonlinear optical parameters, we consider two cases: (a) $\chi_{z''z''z''}^{(2)}=\chi_{z''x''x''}^{(2)}=\chi_{x''z''x''}^{(2)}\neq 0$, $\chi_{x''y''z''}^{(2)}=0$, and (b) $\chi_{z''z''z''}^{(2)}=\chi_{z''x''x''}^{(2)}=\chi_{x''z''x''}^{(2)}=0$, $\chi_{x''y''z''}^{(2)}\neq 0$. Cases (a) and (b) correspond to purely achiral and purely chiral nonlinear optical responses, respectively. We also assume that the crystallographic and particle axes are aligned so that we may use Eq. (33) directly by employing the following relations: $a''/b''=-2$, $a''/c''=-1$, and $d''=0$, corresponding to case (a). Figures 3 and 4 illustrate the effect of sample orientation and input polarization on the radiation patterns. The first column schematically indicates the particle orientation (α,β) while the columns denoted by (a) and (b) display the polar plots of the SH radiation pattern corresponding to cases (a) and (b) above without polarization analysis, i.e., $d\mathcal{P}/d\Omega\propto|E^{(2\omega)}|^2$, along the scattering plane designated by the x-z plane. These figures clearly demonstrate the complex nature of the SH scattering from anisotropic particles such as the effect of the input polarization and particle orientation on the SH radiation pattern, including its magnitude, symmetry, and directionality. In Fig. 3, both the input polarization and the particle axis lie perpendicular to the scattering plane. Consequently, the resulting

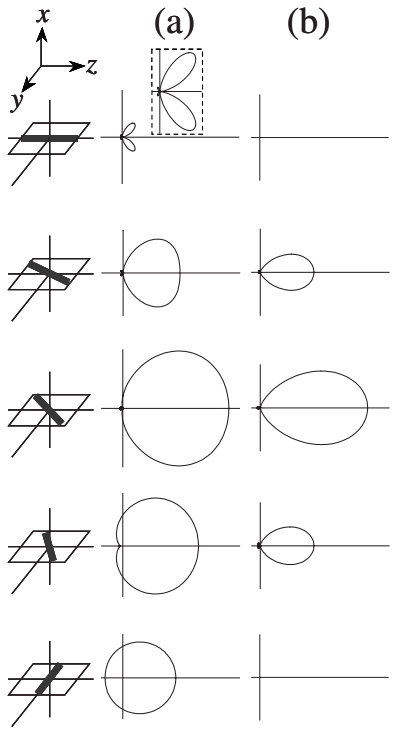

FIG. 3. Radiation patterns for input-field polarization and particle axes both perpendicular to scattering plane defined by the x-z plane ($\hat{\boldsymbol{\epsilon}}_0=\hat{\mathbf{y}}$, $\alpha=\pi/2$) for size parameters $K_1a=1$ and $\Lambda=3$ for a finite cylinder comprised of noncentrosymmetric medium. First column (top to bottom): $\beta=0$, $\pi/8$, $\pi/4$, $3\pi/8$, $\pi/2$. (a) Middle column: $\chi^{(2)}_{z''z''z''}=\chi^{(2)}_{z''x''x''}=\chi^{(2)}_{x''z''x''}\neq 0$ and $\chi^{(2)}_{x''y''z''}=0$; (b) right column: $\chi^{(2)}_{z''z''z''}=\chi^{(2)}_{z''x''x''}=\chi^{(2)}_{x''z''x''}=0$ and $\chi^{(2)}_{x''y''z''}\neq 0$. Inset: magnified view of corresponding plot.

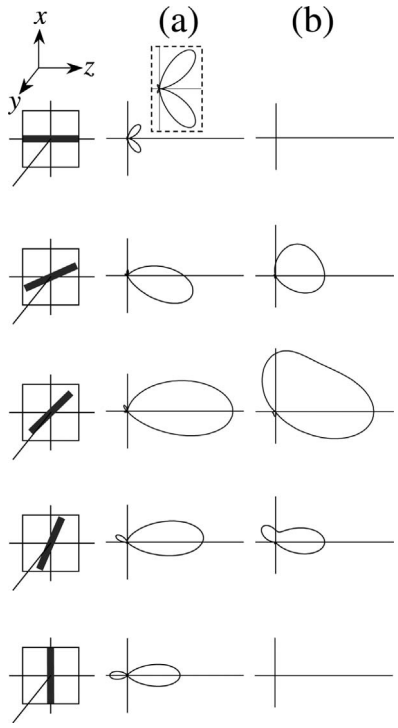

FIG. 4. Radiation patterns using the same geometric, size, and nonlinear optical parameters as in Fig. 3 but with input-field polarization and particle axes both parallel to scattering (x-z) plane ($\hat{\boldsymbol{\epsilon}}_0=\hat{\mathbf{x}}$, $\alpha=0$) for a finite cylinder comprised of noncentrosymmetric medium. (a) Middle column: $\chi^{(2)}_{z''z''z''}=\chi^{(2)}_{z''x''x''}=\chi^{(2)}_{x''z''x''}\neq 0$ and $\chi^{(2)}_{x''y''z''}=0$; (b) right column: $\chi^{(2)}_{z''z''z''}=\chi^{(2)}_{z''x''x''}=\chi^{(2)}_{x''z''x''}=0$ and $\chi^{(2)}_{x''y''z''}\neq 0$. Inset: magnified view of corresponding plot. Note each lower half of the plots corresponds to scattering angles $\varphi=\pi$ and $0\leq\theta\leq\pi$.

radiation patterns are symmetric with respect to the y-z plane. For Fig. 4, both the input polarization and the particle axis lie parallel to the scattering plane resulting in an asymmetric radiation pattern except for particle orientations corresponding to $\beta=0$ or $\pi/2$. For arbitrary particle orientation, the radiation pattern is generally peaked toward the forward scattering direction although backward emission is also possible. This behavior arises mainly from the nature of the linear form factor f whose maximum value occurs in the forward scattering direction ($\mathbf{q}=0$) for a cylindrical particle of arbitrary size according to Eq. (17). Note also in panel (b) of both Figs. 3 and 4 that the forward scattering signal from the chiral contribution peaks when $\beta=\pi/4$ as discussed above.

B. Centrosymmetric case: Surface symmetry classes C_∞, C_6, and C_4

1. Effective susceptibility tensor and associated form factors

For the case of a cylinder comprised of centrosymmetric medium, we consider an isotropic surface lacking mirror plane perpendicular to the surface, corresponding to the symmetry class C_∞, or a surface that exhibits either of the crystalline point group symmetry classes C_4 or C_6, since for these latter two classes, the nonvanishing nonlinear susceptibility elements are identical to those of C_∞ class. To obtain the nonlinear response, we need to express the various components of Eq. (6) or Eq. (26) in terms of the local coordinates of the surface. The surface nonlinear susceptibility elements are given by

$$\chi^{(2)}_{s,\rho'\rho'\rho'},\quad \chi^{(2)}_{s,\rho'\varphi'\varphi'}=\chi^{(2)}_{s,\rho'z'z'},$$
$$\chi^{(2)}_{s,\varphi'\rho'\varphi'}=\chi^{(2)}_{s,z'\rho'z'},\quad \chi^{(2)}_{s,\varphi'z'\rho'}=-\chi^{(2)}_{s,z'\varphi'\rho'}, \tag{34a}$$

$$\chi^{(2)}_{s,z'z'z'},\quad \chi^{(2)}_{s,z'x'x'}=\chi^{(2)}_{s,z'y'y'},$$
$$\chi^{(2)}_{s,x'z'x'}=\chi^{(2)}_{s,y'z'y'},\quad \chi^{(2)}_{s,x'y'z'}=-\chi^{(2)}_{s,y'x'z'}, \tag{34b}$$

for the cylinder's curved surface and flat sides, respectively. Although the indices of the tensor elements may be used to distinguish whether they arise from the curved or flat portion of the cylinder (using cylindrical or Cartesian coordinates, respectively), a possible source of confusion may arise from the term $\chi^{(2)}_{s,z'z'z'}$ for the case of arbitrary surface symmetry since this term is present in both regions of the cylinder; thus, care should be taken when considering the most general symmetry case. This ambiguity may be eliminated by expressing the independent nonlinear susceptibility elements as $\chi^{(2)}_{s,\perp\perp\perp}$, $\chi^{(2)}_{s,\perp\parallel\parallel}$, $\chi^{(2)}_{s,\parallel\perp\parallel}$, and $\chi^{(2)}_{s,\parallel//\perp}$, where $\parallel$ and $\perp$ denote the

TABLE I. Coefficients $\kappa_{ijk,n}$ for the effective susceptibility $\chi_{ijk}^{\text{eff}}=[\sin(Q_3\Lambda a)/(Q_3\Lambda a)]\Sigma_{n=0}^{3}\kappa_{ijk,n}J_n(\delta_0)/\delta_0^n$ of a finite cylinder of radius a and length L, comprised of centrosymmetric medium with isotropic surface lacking mirror symmetry, where $\Lambda=L/2a$, $\delta_0=Qa$, $\chi_1=3\chi_{s,\perp\perp\perp}^{(2)}+\chi_{s,\perp\parallel\parallel}^{(2)}+2\chi_{s,\parallel\perp\parallel}^{(2)}+4\gamma$, $\chi_2=\chi_{s,\perp\perp\perp}^{(2)}+3\chi_{s,\perp\parallel\parallel}^{(2)}-2\chi_{s,\parallel\perp\parallel}^{(2)}+4\gamma$, and $\chi_3=\chi_{s,\perp\perp\perp}^{(2)}-\chi_{s,\perp\parallel\parallel}^{(2)}-2\chi_{s,\parallel\perp\parallel}^{(2)}$. Indices ijk of κ are suppressed for simplicity.

ijk	κ_0	κ_1	κ_2	κ_3
$x'x'x'$		$(i/2)Q_1\chi_1$		$-(i/2)(Q_1^3-3Q_1Q_2^2)a^2\chi_3$
$x'x'y'$		$(i/4)Q_2(\chi_1-\chi_2)$		$(i/2)(Q_2^3-3Q_2Q_1^2)a^2\chi_3$
$x'x'z'$		$2iQ_3\chi_{s,\parallel\perp\parallel}^{(2)}$	$2Q_1Q_2a\chi_{s,\parallel//\perp}^{(2)}$	
$x'y'y'$		$(i/2)Q_1\chi_2$		$(i/2)(Q_1^3-3Q_1Q_2^2)a^2\chi_3$
$x'y'z'$	$-\chi_{s,\parallel//\perp}^{(2)}/a$	$2iQ_3\chi_{s,\parallel//\perp}^{(2)}$	$-(Q_1^2-Q_2^2)a\chi_{s,\parallel//\perp}^{(2)}$	
$x'z'z'$		$2iQ_1(\chi_{s,\perp\parallel\parallel}^{(2)}+\gamma)$		
$y'x'x'$		$(i/2)Q_2\chi_2$		$(i/2)(Q_2^3-3Q_2Q_1^2)a^2\chi_3$
$y'x'y'$		$(i/4)Q_1(\chi_1-\chi_2)$		$(i/2)(Q_1^3-3Q_1Q_2^2)a^2\chi_3$
$y'x'z'$	$\chi_{s,\parallel//\perp}^{(2)}/a$	$-2iQ_3\chi_{s,\parallel//\perp}^{(2)}$	$-(Q_1^2-Q_2^2)a\chi_{s,\parallel//\perp}^{(2)}$	
$y'y'y'$		$(i/2)Q_2\chi_1$		$-(i/2)(Q_2^3-3Q_2Q_1^2)a^2\chi_3$
$y'y'z'$		$2iQ_3\chi_{s,\parallel\perp\parallel}^{(2)}$	$-2Q_1Q_2a\chi_{s,\parallel//\perp}^{(2)}$	
$y'z'z'$		$2iQ_2(\chi_{s,\perp\parallel\parallel}^{(2)}+\gamma)$		
$z'x'x'$		$2iQ_3(\chi_{s,\perp\parallel\parallel}^{(2)}+\gamma)$	$-4Q_1Q_2a\chi_{s,\parallel//\perp}^{(2)}$	
$z'x'y'$			$2(Q_1^2-Q_2^2)a\chi_{s,\parallel//\perp}^{(2)}$	
$z'x'z'$		$2iQ_1\chi_{s,\parallel\perp\parallel}^{(2)}$		
$z'y'y'$		$2iQ_3(\chi_{s,\perp\parallel\parallel}^{(2)}+\gamma)$	$4Q_1Q_2a\chi_{s,\parallel//\perp}^{(2)}$	
$z'y'z'$		$2iQ_2\chi_{s,\parallel\perp\parallel}^{(2)}$		
$z'z'z'$		$2iQ_3(\chi_{s,\perp\parallel\parallel}^{(2)}+\gamma)$		

local coordinates parallel and perpendicular to the surface. The symbol // is used in addition to the symbol ∥ to distinguish between the two orthogonal coordinates parallel to the surface. We employ these symbols to describe the local coordinates from either the flat or curved portions of the cylinder. The susceptibility element $\chi_{s,\parallel//\perp}^{(2)}$ is the chiral term, and, if $\{\parallel,//,\perp\}$ forms a right-handed coordinate system, $\chi_{s,\parallel//\perp}^{(2)}=-\chi_{s,//\parallel\perp}^{(2)}$. Compiling the contributions from Eqs. (25), (27), and (28), we obtain $p_i'=\chi_{ijk}^{\text{eff}}\mathcal{E}_j\mathcal{E}_k$, where χ_{ijk}^{eff} is the effective nonlinear susceptibility, which may be written as

$$\chi_{ijk}^{\text{eff}}=\frac{\sin(Q_3\Lambda a)}{Q_3\Lambda a}\sum_{n=0}^{3}\kappa_{ijk,n}\frac{J_n(\delta_0)}{\delta_0^n}. \tag{35}$$

The coefficients $\kappa_{ijk,n}$ are presented in Table I. By comparison of Eq. (35) with Eq. (19), the products $f_n=[\sin(Q_3\Lambda a)/(Q_3\Lambda a)][2^n n!J_n(\delta_0)/\delta_0^n]$, where $n=0$, 1, 2, and 3, may be defined, albeit somewhat arbitrary, as the various "linear" form factors responsible for SH scattering from finite cylinders comprised of centrosymmetric media. Note that an extra factor of $2^n n!$ is included in the definition of f_n so that in the limit as $\mathbf{q}\to 0$, f_n approaches unity as in the case of the linear optical form factor defined in Eq. (17). The form factor f_n is further modified by the coefficient $\kappa_{ijk,n}$ that is a linear combination of $(Q_m a)^n$ where $m=1$, 2, or 3.

Despite the assumption of a general isotropic surface that lacks mirror symmetry, where only four independent surface nonlinear susceptibility elements exist as listed in Eqs. (34a) and (34b), Table I reveals that all 18 effective susceptibility tensor elements are nonvanishing and independent. This result is noteworthy since for the case of a sphere comprised of centrosymmetric medium with *arbitrary* surface symmetry, only four effective susceptibility elements are nonvanishing and independent, as obtained in Appendix B. These four elements, denoted by $\tilde{\chi}_{ijk}^{\text{eff}}$ for the sphere, are listed in Table II. For the corresponding case of SFG from a sphere comprised of centrosymmetric medium, seven independent effective susceptibilities are nonvanishing, which arise from 27 independent surface susceptibility components.[54] When Kleinman symmetry is valid and $\gamma=0$, it can be shown by inspection of Table I that the number of effective susceptibility elements for SHG reduces from 18 to 9 and, in addition, the effective susceptibility elements themselves obey the Kleinman symmetry condition, i.e., the interchange of indices does not alter the effective susceptibility element. In comparison, for the case of a sphere of centrosymmetric medium, when $\gamma=0$ and the surface nonlinear susceptibility elements obey the Kleinman symmetry condition, the resulting number of effective nonlinear susceptibility elements reduces from four to two, with the elements themselves also obeying the Kleinman symmetry condition. The large disparity in the number of effective nonlinear optical susceptibility elements between the cylinder and the sphere is clearly indicative of the strong effect of the intrinsic anisotropy of the cylinder.

2. Source and emission characteristics

We now briefly comment on the source and emission characteristics of the SH scattering process from cylinders.

TABLE II. Coefficients $\tilde{\kappa}_{ijk,n}$ of the effective susceptibility, $\tilde{\chi}^{\text{eff}}_{ijk}=\Sigma_{n=0}^{3}\tilde{\kappa}_{ijk,n}J_{(n+1)/2}(\delta)/\delta^{(n+1)/2}$, of a sphere of radius a comprised of centrosymmetric medium with arbitrary surface symmetry, where $\delta=qa$, $\tilde{\chi}_{11}=\chi^{(2)}_{s,r'r'r'}-\chi^{(2)}_{s,r'\theta'\theta'}-2\chi^{(2)}_{s,\theta'r'\theta'}$, $\tilde{\chi}_{12}=\chi^{(2)}_{s,\theta'\theta'r'}+\chi^{(2)}_{s,\varphi'\varphi'r'}$, $\tilde{\chi}_{13}=\chi^{(2)}_{s,r'\theta'\theta'}+\chi^{(2)}_{s,r'\varphi'\varphi'}+2\gamma$, $\tilde{\chi}_{21}=\chi^{(2)}_{s,\theta'\theta'\theta'}-\chi^{(2)}_{s,\theta'r'r'}-2\chi^{(2)}_{s,r'\theta'r'}$, $\tilde{\chi}_{22}=\chi^{(2)}_{s,\varphi'\theta'\varphi'}+\chi^{(2)}_{s,r'\theta'r'}$, $\tilde{\chi}_{23}=\chi^{(2)}_{s,\theta'\varphi'\varphi'}+\chi^{(2)}_{s,\theta'r'r'}$, $\tilde{\chi}_{31}=\chi^{(2)}_{s,\theta'\varphi'r'}-\chi^{(2)}_{s,\varphi'\theta'r'}$, $\tilde{\chi}_{32}=2\chi^{(2)}_{s,\varphi'\theta'r'}-\chi^{(2)}_{s,\theta'\varphi'r'}-\chi^{(2)}_{s,r'\theta'\varphi'}$, and $\tilde{\chi}_{33}=-\chi^{(2)}_{s,\theta'\theta'\varphi'}+\chi^{(2)}_{s,\varphi'\theta'\theta'}-\chi^{(2)}_{s,\varphi'r'r'}+\chi^{(2)}_{s,r'\varphi'r'}$. Indices ijk of $\tilde{\kappa}$ are suppressed for simplicity. Note $\tilde{\chi}^{\text{eff}}_{x'y'z'}=-\tilde{\chi}^{\text{eff}}_{y'x'z'}$.

ijk	$\tilde{\kappa}_0$	$\tilde{\kappa}_1$	$\tilde{\kappa}_2$	$\tilde{\kappa}_3$
$x'z'x'$, $y'z'y'$	$(-3i/a)\sqrt{\pi/2}\,\tilde{\chi}_{11}/\delta$	$-3\pi(\tilde{\chi}_{21}+\tilde{\chi}_{22})/(4a)$	$(3i/2a)\sqrt{\pi/2}\,(6\tilde{\chi}_{11}+\tilde{\chi}_{12}\delta^2)/\delta$	$9\pi\tilde{\chi}_{21}/(4a)$
$z'x'x'$, $z'y'y'$	$(-3i/a)\sqrt{\pi/2}\,\tilde{\chi}_{11}/\delta$	$-3\pi(\tilde{\chi}_{21}+\tilde{\chi}_{23})/(4a)$	$(3i/2a)\sqrt{\pi/2}\,(6\tilde{\chi}_{11}+\tilde{\chi}_{13}\delta^2)/\delta$	$9\pi\tilde{\chi}_{21}/(4a)$
$z'z'z'$	$(6i/a)\sqrt{\pi/2}\,\tilde{\chi}_{11}/\delta$	$3\pi(\tilde{\chi}_{21}-\chi^{(2)}_{s,\theta'\theta'\theta'})/(2a)$	$(-3i/a)\sqrt{\pi/2}\,(6\tilde{\chi}_{11}-\chi^{(2)}_{s,r'r'r'}\delta^2)/\delta$	$-9\pi\tilde{\chi}_{21}/(2a)$
$x'y'z'$, $(-)y'x'z'$	$(3/2a)\sqrt{\pi/2}\,\tilde{\chi}_{31}$		$(3/a)\sqrt{\pi/2}\,\tilde{\chi}_{32}$	$3\pi i\delta\tilde{\chi}_{33}/(4a)$

The observations we state here are valid not only for the general isotropic surface described above but also for the case of arbitrary surface symmetry. All of the 18 independent effective nonlinear susceptibility elements are nonvanishing, and may be expressed in terms of both the wave-vector transfer factors Q_i and the Bessel functions $J_n(\delta_0)$. The contributions from the curved and flat portions of the cylinder, which may be distinguished by the presence of the coefficient Q_i ($i=1$ or 2 for the curved region and $i=3$ for the flat sides), have different emission characteristics. In particular, the surface nonlinear polarization from the flat sides radiates only with the form factor $f_1\propto J_1(\delta_0)$, as in the case of a cylinder comprised of noncentrosymmetric medium. In contrast, the nonlinear optical sources from the curved surface may experience multiple form factors proportional to $J_0(\delta_0)$, $J_1(\delta_0)$, $J_2(\delta_0)$, or $J_3(\delta_0)$. The contribution from the nonlocal bulk susceptibility γ is found to radiate only with the form factor $f_1\propto J_1(\delta_0)$. It has been shown previously that the term γ may be represented by an equivalent surface nonlinear optical susceptibility with nonvanishing components $(\chi^{(2)}_{s,\gamma})_{\perp\perp\perp}=(\chi^{(2)}_{s,\gamma})_{\perp\parallel\parallel}=\gamma$.[6,86] Thus, in evaluating the total nonlinear form factor $\mathbf{p}=\mathbf{p}_s+\mathbf{p}_b$ [Eq. (24)], one needs only to calculate $\mathbf{p}_s$, and then make the replacements $\chi^{(2)}_{s,\perp\perp\perp}\rightarrow\chi^{(2)}_{s,\perp\perp\perp}+\gamma$ and $\chi^{(2)}_{s,\perp\parallel\parallel}\rightarrow\chi^{(2)}_{s,\perp\parallel\parallel}+\gamma$, in order to take into account the bulk term γ. As a consequence, the nonlocal bulk term γ contributes only to nine effective susceptibility elements of the form χ^{eff}_{ijj} according to Eq. (25). The bulk-surface inseparability of the γ and the surface nonlinear susceptibilities $\chi^{(2)}_{s,\perp\perp\perp}$ and $\chi^{(2)}_{s,\perp\parallel\parallel}$ is reflected in Tables I–III.

3. Radiation patterns: Examples

Using the same dimensions of the cylinder presented in Figs. 3 and 4 for the case of noncentrosymmetric medium, we now plot the corresponding SH radiation patterns in Figs. 5 and 6 for the case of centrosymmetric medium. For illustration purposes as well as a comparison with the noncentrosymmetric cases discussed above, we assume the following sets of the surface nonlinear optical parameters: (a) $\chi^{(2)}_{s,\perp\perp\perp}=\chi^{(2)}_{s,\perp\parallel\parallel}=\chi^{(2)}_{s,\parallel\perp\parallel}\neq 0$, $\chi^{(2)}_{s,\parallel//\perp}=0$, $\gamma=0$ and (b) $\chi^{(2)}_{s,\perp\perp\perp}=\chi^{(2)}_{s,\perp\parallel\parallel}=\chi^{(2)}_{s,\parallel\perp\parallel}=0$, $\chi^{(2)}_{s,\parallel//\perp}\neq 0$, $\gamma=0$, to illustrate cases with pure achiral and chiral responses, respectively. Figures 5 and 6 display the SH radiation patterns without polarization analysis corresponding to the cases (a) and (b) above as a function of the particle orientation using the same input-polarization conditions employed in Figs. 3 and 4. Note, as in Fig. 3, the resulting radiation patterns in Fig. 5 are symmetric with respect to the y-z plane, while, as in Fig. 4, the radiation patterns in Fig. 6 for particle orientations corresponding to $\beta\neq 0$ or $\pi/2$ are asymmetric. In contrast to the noncentrosymmetric case where forward emission dominates, for arbitrary particle orientation, the achiral suscepti-

TABLE III. Effective susceptibility elements, χ^{eff}_{ijk}, for a small (Rayleigh limit) finite cylinder comprised of centrosymmetric medium with arbitrary surface symmetry, where $\chi_{11}=(3\chi^{(2)}_{s,\rho'\rho'\rho'}+\chi^{(2)}_{s,\rho'\varphi'\varphi'}+2\chi^{(2)}_{s,\rho'\rho'\varphi'}+4\gamma)$, $\chi_{12}=(\chi^{(2)}_{s,\rho'\rho'\rho'}+3\chi^{(2)}_{s,\rho'\varphi'\varphi'}-2\chi^{(2)}_{s,\rho'\rho'\varphi'}+4\gamma)$, $\chi_{21}=(\chi^{(2)}_{s,\varphi'\varphi'\varphi'}+3\chi^{(2)}_{s,\varphi'\rho'\rho'}-2\chi^{(2)}_{s,\rho'\rho'\varphi'})$, and $\chi_{22}=(3\chi^{(2)}_{s,\varphi'\varphi'\varphi'}+\chi^{(2)}_{s,\varphi'\rho'\rho'}+2\chi^{(2)}_{s,\rho'\rho'\varphi'})$. Only the contributions from the curved part of the cylinder are explicitly shown since the contributions from its circular caps and the associated bulk component γ are expressed simply as $i(\chi^{(2)}_{s,ijk}+\gamma\delta_{i3}\delta_{jk})Q_3$. The terms χ^{FE}_{ijk} are defined in Eqs. (36a)–(36d).

ijk	$\chi^{\text{eff}}_{ijk}-i(\chi^{(2)}_{s,ijk}+\gamma\delta_{i3}\delta_{jk})Q_3$
$x'x'x'$	$(i/4)[\chi_{11}Q_1-\chi_{22}Q_2]$
$x'x'y'$	$(i/8)[(\chi_{22}-\chi_{21})Q_1+(\chi_{11}-\chi_{12})Q_2]$
$x'x'z'$	$\chi^{\text{FE}}_{x'x'z'}$
$x'y'y'$	$(i/4)[\chi_{12}Q_1-\chi_{21}Q_2]$
$x'y'z'$	$\chi^{\text{FE}}_{x'y'z'}$
$x'z'z'$	$i[(\chi^{(2)}_{s,\rho'z'z'}+\gamma)Q_1-\chi^{(2)}_{s,\varphi'z'z'}Q_2]$
$y'x'x'$	$(i/4)[\chi_{21}Q_1+\chi_{12}Q_2]$
$y'x'y'$	$(i/8)[(\chi_{11}-\chi_{12})Q_1-(\chi_{22}-\chi_{21})Q_2]$
$y'x'z'$	$\chi^{\text{FE}}_{y'x'z'}=-\chi^{\text{FE}}_{x'y'z'}$
$y'y'y'$	$(i/4)[\chi_{22}Q_1+\chi_{11}Q_2]$
$y'y'z'$	$\chi^{\text{FE}}_{y'y'z'}=\chi^{\text{FE}}_{x'x'z'}$
$y'z'z'$	$i[\chi^{(2)}_{s,\varphi'z'z'}Q_1+(\chi^{(2)}_{s,\rho'z'z'}+\gamma)Q_2]$
$z'x'x'$	$\chi^{\text{FE}}_{z'x'x'}$
$z'x'y'$	$\chi^{FE}_{z'x'y'}=0$
$z'x'z'$	$i(\chi^{(2)}_{s,z'\rho'z'}Q_1-\chi^{(2)}_{s,z'\varphi'z'}Q_2)$
$z'y'y'$	$\chi^{\text{FE}}_{z'y'y'}=\chi^{\text{FE}}_{z'x'x'}$
$z'y'z'$	$i(\chi^{(2)}_{s,z'\varphi'z'}Q_1+\chi^{(2)}_{s,z'\rho'z'}Q_2)$
$z'z'z'$	$\chi^{\text{FE}}_{z'z'z'}$

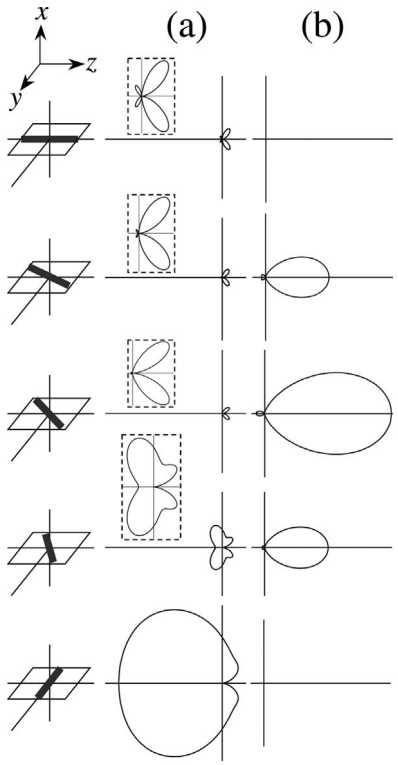

FIG. 5. Radiation patterns for input-field polarization and particle axes both perpendicular to scattering plane defined by the x-z plane ($\hat{\boldsymbol{\epsilon}}_0=\hat{\mathbf{y}}$, $\alpha=\pi/2$) for size parameters $K_1a=1$ and $\Lambda=3$ for a finite cylinder comprised of centrosymmetric medium. First column (top to bottom): $\beta=0$, $\pi/8$, $\pi/4$, $3\pi/8$, $\pi/2$. (a) Middle column, $\chi^{(2)}_{s,z''z''z''}=\chi^{(2)}_{s,z''x''x''}=\chi^{(2)}_{s,x''z''x''}\neq 0$, $\chi^{(2)}_{s,x''y''z''}=0$, and $\gamma=0$; (b) right column, $\chi^{(2)}_{s,z''z''z''}=\chi^{(2)}_{s,z''x''x''}=\chi^{(2)}_{s,x''z''x''}=0$, $\chi^{(2)}_{s,x''y''z''}\neq 0$, and $\gamma=0$. Insets: magnified views of corresponding plots.

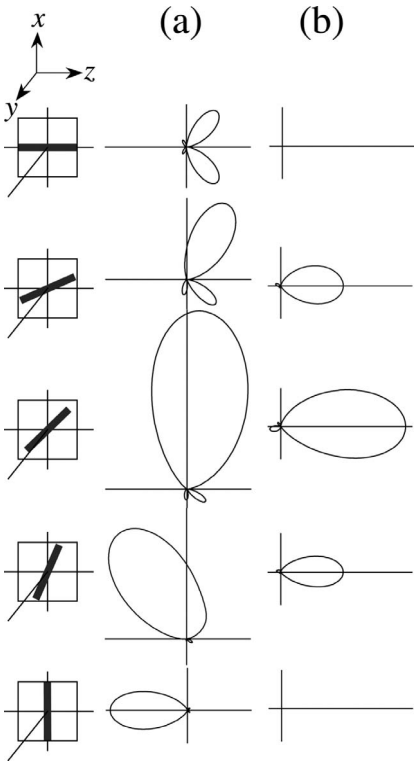

FIG. 6. Radiation patterns using the same geometric, size, and nonlinear optical parameters as in Fig. 5 but with input-field polarization and particle axes both parallel to scattering (x-z) plane ($\hat{\boldsymbol{\epsilon}}_0=\hat{\mathbf{x}}$, $\alpha=0$) for a finite cylinder comprised of centrosymmetric medium. (a) Middle column: $\chi^{(2)}_{s,z''z''z''}=\chi^{(2)}_{s,z''x''x''}=\chi^{(2)}_{s,x''z''x''}\neq 0$, $\chi^{(2)}_{s,x''y''z''}=0$, and $\gamma=0$; (b) right column: $\chi^{(2)}_{s,z''z''z''}=\chi^{(2)}_{s,z''x''x''}=\chi^{(2)}_{s,x''z''x''}=0$, $\chi^{(2)}_{s,x''y''z''}\neq 0$, and $\gamma=0$. Note each lower half of the plots corresponds to scattering angles $\varphi=\pi$ and $0\leq\theta\leq\pi$.

bility elements $\chi^{(2)}_{s,\perp\perp\perp}$, $\chi^{(2)}_{s,\perp\parallel\parallel}$, and $\chi^{(2)}_{s,\parallel\perp\parallel}$ do not radiate in the forward direction, as shown in column (a) of Figs. 5 and 6. This property may also be seen directly from Table I: For the achiral response, the leading-order contribution to the SHG signal corresponds to $\kappa_{ijk,1}\propto Q_m$ ($m=1,2$, or 3), which vanishes in the forward direction. In addition, relatively strong backward emission, for example, is observed for $\beta=\pi/2$ for this size parameter considered. The chiral component $\chi^{(2)}_{s,\parallel//\perp}$, on the other hand, yields prominent emission in the forward direction as we have shown above.

C. Special geometries

An examination of the nonlinear form factor in Eq. (6) reveals that pertinent limiting cases become apparent by considering the condition $\mathbf{q}\cdot\mathbf{r}'\ll 1$, which may be satisfied by employing the forward scattering geometry ($\mathbf{q}=0$) or by probing small particles such that $r'\ll q^{-1}_{\max}$, where $q_{\max}=2K_1$. In the discussions below, we assume all 18 independent nonlinear susceptibility elements to be nonvanishing for both noncentrosymmetric and centrosymmetric media.

1. Forward scattering: $\mathbf{q}=0$

Let us first consider the case of noncentrosymmetric medium. In the forward direction, recall that $f=1$, hence $\mathbf{p}=\boldsymbol{\chi}_0$ using Eq. (16). We see from this simple result that the maximum signal is expected for the forward scattering geometry. The measured SH signal in the forward scattering direction is ultimately determined by the term $\boldsymbol{\chi}_0$ according to Eq. (18), i.e., the crystallographic orientation of the particle and the polarization state of the fundamental field. It should be noted, however, that the condition $f\approx 1$ is also possible at other scattering directions, in particular, when the particle dimensions are much smaller than the wavelength of light; this case is discussed in Sec. III C 2. The condition $f=1$ (or $f\approx 1$ for small particles in the Rayleigh limit) provides a convenient means of probing or deducing the crystallographic directions without interference effects. These effects occur, for example, when SH signals are recorded at directions away from the forward scattering direction. In addition, they arise from the part of the form factor associated with the length of the cylinder, i.e., $\sin(Q_3\Lambda a)/(Q_3\Lambda a)=\mathrm{sinc}(Q_3\Lambda a)$, which is an oscillatory function of $(Q_3\Lambda a)$. This characteristic behavior is in accord with a recent experimental SH study, which reported the observation of decreasing number of fringes as the length of a cylindrical particle is reduced.[44] Note further that the nonlinear form factor for the centrosymmetric case also depends on $\mathrm{sinc}(Q_3\Lambda a)$ through Eqs. (25), (27), and (28), which underscores the effect of a cylinder's finite length on its nonlinear optical response.

TABLE IV. Leading-order scaling of SH field $E^{(2\omega)}$ for small particles in the Rayleigh limit. Note V denotes the volume of the particle, and $A \propto aL$ and a^2 for the cylinder and sphere, respectively. The forward emitting surface nonlinear optical susceptibility elements are presented in Sec. III C 1.

Bulk symmetry	Shape	$E^{(2\omega)}$	Sources
Noncentrosymmetric	Cylinder, sphere	V/λ^2	Bulk $\chi^{(2)}_{ijk}$
Centrosymmetric	Cylinder	A/λ^2	Forward emitting $\chi^{(2)}_{s,ijk}$
		V/λ^3	Nonforward emitting $\chi^{(2)}_{s,ijk}$, bulk γ
	Sphere	A/λ^2	Nonisotropic $\chi^{(2)}_{s,ijk}$
		V/λ^3	Isotropic (achiral) $\chi^{(2)}_{s,ijk}$, bulk γ
		A^2/λ^4	Isotropic (chiral) $\chi^{(2)}_{s,ijk}$

The case of the centrosymmetric medium is more complex compared to the noncentrosymmetric case. Consider the various components of $\mathbf{p}=\mathbf{p}_s^{\text{flat}}+\mathbf{p}_s^{\text{curved}}+\mathbf{p}_b$. In the forward direction, $\mathbf{p}_b=\mathbf{p}_s^{\text{flat}}=0$ since $\mathbf{q}=0$, as seen in Eqs. (25) and (27). The remaining contribution, $\mathbf{p}_s^{\text{curved}}$, is evaluated by using the terms I_n defined in Eqs. (30a)–(30d). For $\mathbf{q}=0$ and using the properties of $J_n(u)$ as $u\rightarrow 0$, i.e., $J_n(u) \approx (u^n/2^n n!)$, we obtain $I_0=2\pi$, $I_1=0$, $I_2=(A_1A_2+B_1B_2)\pi$, and $I_3=0$. The nonvanishing terms I_0 and I_2 correspond to the following eight independent nonlinear susceptibility elements with indices given by $\rho'\rho'z'$, $\varphi'\rho'z'$, $\rho'\varphi'z'$, $\varphi'\varphi'z'$, $z'\rho'\rho'$, $z'\varphi'\varphi'$, $z'\rho'\varphi'$, and $z'z'z'$. Of these eight terms, the contribution due to the component $\chi^{(2)}_{s,z'\rho'\varphi'}$ vanishes upon evaluation of Eq. (29), thus leaving seven susceptibility elements that may give rise to forward emission; its contribution to the corresponding SFG process, however, is nonvanishing. To understand the physical significance of these surface susceptibility terms, we evaluate $\mathbf{p}$ for the forward scattering geometry, for which we obtain $p_i'=\chi^{\text{FE}}_{ijk}\mathcal{E}_j\mathcal{E}_k$, where χ^{FE}_{ijk} is the effective nonlinear susceptibility tensor element responsible for SH forward emission. Explicitly,

$$\chi^{\text{FE}}_{z'z'z'} = \frac{2}{a}\chi^{(2)}_{s,z'z'z'}, \tag{36a}$$

$$\chi^{\text{FE}}_{z'x'x'} = \chi^{\text{FE}}_{z'y'y'} = \frac{1}{a}(\chi^{(2)}_{s,z'\rho'\rho'} + \chi^{(2)}_{s,z'\varphi'\varphi'}), \tag{36b}$$

$$\chi^{\text{FE}}_{x'x'z'} = \chi^{\text{FE}}_{y'y'z'} = \frac{1}{a}(\chi^{(2)}_{s,\rho'\rho'z'} + \chi^{(2)}_{s,\varphi'\varphi'z'}), \tag{36c}$$

$$\chi^{\text{FE}}_{x'y'z'} = -\chi^{\text{FE}}_{y'x'z'} = \frac{1}{a}(\chi^{(2)}_{s,\rho'\varphi'z'} - \chi^{(2)}_{s,\varphi'\rho'z'}). \tag{36d}$$

Thus, in the forward scattering direction, the seven special surface nonlinear susceptibility elements above give rise to an effective nonlinear susceptibility tensor having four independent elements, which resembles the nonlinear optical response of a material system possessing C_∞ symmetry. The four terms in Eqs. (36a)–(36d) are analogous to the bulk nonlinear susceptibility elements in Eq. (32). Note that for forward emission, the SH radiation arises from the curved portion of the cylinder. Note further that the corresponding set of susceptibilities residing in the flat portions of the cylinder do not give rise to forward emission since $Q_3=0$, as can be seen from Eq. (27).

2. Rayleigh particles, wires, and disks

To describe the nonlinear optical response of a small particle in the Rayleigh limit, with a and $L \ll \lambda$, one may employ the properties of $J_n(u)$ and $\sin u/u$ for small arguments ($u \ll 1$). For both cases of noncentrosymmetric and centrosymmetric media, the nonlinear form factor $\mathbf{p}^{\text{Rayleigh}}$ may be expressed in terms of the effective susceptibility χ^{eff}_{ijk} with respect to the particle frame, and its ith component is given by

$$p_i'^{\text{Rayleigh}} = \chi^{\text{eff}}_{ijk}\mathcal{E}_j\mathcal{E}_k. \tag{37}$$

For the noncentrosymmetric medium, $f \approx 1$; thus, using Eq. (23), we obtain $\chi^{\text{eff}}_{ijk}=\chi'^{(2)}_{ijk}=\chi^{(2)}_{lmn}M''_{li}M''_{mj}M''_{nk}$, and in addition, the maximum possible signal is no longer restricted to forward scattering as seen in larger particles. Thus, the scattering efficiency in other directions (including backscattering) increases as the dimensions decrease, and the signal strength depends on the crystallographic orientation, the polarization conditions, as well as the scattering direction since $\mathbf{p} \approx \boldsymbol{\chi}_0$. For the case of centrosymmetric medium with arbitrary surface symmetry, the various elements of $\boldsymbol{\chi}^{\text{eff}}$ are listed in Table III. The element χ^{eff}_{ijk} depends on both the scattering directions and the particle's orientation through $Q_i=M'_{ij}q_j$. There are 18 independent and nonvanishing effective susceptibility elements that arise from the flat surfaces of the cylinder, and are evaluated to be $i(\chi^{(2)}_{s,ijk}+\gamma\delta_{i3}\delta_{jk})Q_3$, for all (i,j,k). Thus we show explicitly only the contributions from the curved surface in Table III. For the case of a small sphere in the Rayleigh limit, comprised of centrosymmetric medium, one may show using Table II that the number of independent effective susceptibility elements $\tilde{\chi}^{\text{eff}}_{ijk}$ remains four.

We now consider how the SH field scales with the dimensions and wavelength for small finite cylinders and spheres in the Rayleigh limit. In the discussion below, V denotes the volume of the particle, and A refers to either the area of the cylindrical wall or the total area for the case of the cylinder or sphere, respectively. The results are summarized in Table IV. According to Eq. (7), the SH field magnitude is proportional to $\sim K^2Vp$ where p is the magnitude of the nonlinear form factor. For a small particle of noncentrosymmetric medium, $p \approx |\boldsymbol{\chi}_0|$. Consequently, for a cylinder or a sphere, $E^{(2\omega)} \sim V/\lambda^2$, which is the same as the scaling for linear op-

tical scattering for small cylinders or spheres. For a small cylinder of centrosymmetric medium, an inspection of Table III and Eq. (36) reveals that the SH field scales either as $\sim V/\lambda^3$ or $\sim A/\lambda^2$, depending on the type of surface nonlinear optical source. The scaling corresponding to $E^{(2\omega)} \sim V/\lambda^3$ originates from the set of nonlinear susceptibilities that do not contribute to forward emission. The scaling corresponding to $E^{(2\omega)} \sim A/\lambda^2$ is obtained when one of the nonlinear susceptibilities responsible for the SH forward scattering is present, e.g., the surface chiral susceptibility $\chi^{(2)}_{s,\parallel//\perp}$. For a small sphere of centrosymmetric medium, a similar behavior to that of a cylinder is obtained, wherein two distinct groups of nonlinear susceptibility elements yield different responses. In the limit of $a \ll \lambda$ in Table II, one may show that for a sphere possessing a general isotropic surface whose nonlinear susceptibility elements are $\chi^{(2)}_{s,\perp\perp\perp}$, $\chi^{(2)}_{s,\perp\parallel\parallel}$, $\chi^{(2)}_{s,\parallel\perp\parallel}$, and $\chi^{(2)}_{s,\parallel//\perp} = -\chi^{(2)}_{s,//\parallel\perp}$, the SH field scales as $E^{(2\omega)} \sim V/\lambda^3$. This result has also been proven for arbitrary index mismatch in Ref. 23. For this leading-order term, the isotropic chiral contribution vanishes, but its lowest-order contribution to the SH signal corresponds to the scaling $E^{(2\omega)} \sim (A/\lambda^2)^2$. For nonisotropic sources, the field scales as $E^{(2\omega)} \sim A/\lambda^2$. We now summarize the results for cylinders and spheres comprised of centrosymmetric medium in terms of two relevant observations. First, the small-particle scaling of the field $E^{(2\omega)}$ depends on the surface symmetry. For example, a seemingly simple system such as the small sphere may exhibit field dependence $E^{(2\omega)} \sim (A/\lambda^2)$ when the surface is locally anisotropic, instead of the expected $E^{(2\omega)} \sim V/\lambda^3$, when the surface is locally isotropic. The second observation pertains to the response of small cylinders and spheres that possess isotropic surfaces: For the case of the cylinder, $E^{(2\omega)} \sim (A/\lambda^2)$, which is dominated by the surface chiral susceptibility $\chi^{(2)}_{s,\parallel//\perp}$, whereas for the sphere, $E^{(2\omega)} \sim V/\lambda^3$, which is dominated by the surface achiral sources $\chi^{(2)}_{s,\perp\perp\perp}$, $\chi^{(2)}_{s,\perp\parallel\parallel}$, and $\chi^{(2)}_{s,\parallel\perp\parallel}$.

For the case of wires or disks, one may also obtain simplified expressions for the nonlinear form factor. For wires with $a \ll \lambda$ and arbitrary length L, we have

$$\mathbf{p}^{\text{wire}} = \frac{\sin(Q_3 \Lambda a)}{Q_3 \Lambda a} \mathbf{p}^{\text{Rayleigh}}. \tag{38}$$

The vector $\mathbf{p}^{\text{Rayleigh}}$ is given by Eq. (37). For noncentrosymmetric medium, the effective susceptibility is given by $\chi^{\text{eff}}_{ijk} = \chi^{(2)}_{lmn} M''_{li} M''_{mj} M''_{nk}$; for centrosymmetric medium, χ^{eff}_{ijk} is given by Table III. For the case of disks, where $L \ll \lambda$ and a is arbitrary, the term $\sin(Q_3 \Lambda a)/(Q_3 \Lambda a) \approx 1$ so that the nonlinear form factor becomes

$$\mathbf{p}^{\text{disk}} = \frac{2J_1(Qa)}{Qa} \boldsymbol{\chi}_0, \tag{39a}$$

$$\mathbf{p}^{\text{disk}} = i[\gamma(\hat{\boldsymbol{\epsilon}}_0 \cdot \hat{\boldsymbol{\epsilon}}_0)\mathbf{q} + Q_3 \vec{\vec{\chi}}^{(2)}_s : \hat{\boldsymbol{\epsilon}}_0 \hat{\boldsymbol{\epsilon}}_0] \frac{2J_1(Qa)}{Qa} + \frac{\boldsymbol{\Gamma}}{\pi a} \tag{39b}$$

for (a) noncentrosymmetric and (b) centrosymmetric media, respectively.

D. Role of surface chirality

We now discuss a topic of considerable significance: the chiral nature of the surface nonlinear optical response.[87–92] Let us first examine the case of a cylinder comprised of centrosymmetric medium with an isotropic surface lacking mirror symmetry, which we have considered in Sec. III B above. By inspection of Table I, we find that the "chiral" effective susceptibility elements having indices $x'y'z'$, $y'z'x'$, and $z'x'y'$ are derived purely from the chiral surface susceptibility element $\chi^{(2)}_{s,\parallel//\perp}$. In contrast to the case of the sphere of centrosymmetric medium, this specific set of effective susceptibilities does not obey the standard chiral symmetry rules for SHG within the dipole approximation, given by

$$\chi^{\text{eff}}_{x'y'z'} = -\chi^{\text{eff}}_{y'x'z'}, \quad \chi^{\text{eff}}_{z'x'y'} = 0. \tag{40}$$

When $Q_1 = \pm Q_2$, Eq. (40) is obeyed and an effective chiral axis is established along the particle axis $\hat{\mathbf{z}}'$. The condition $Q_1 = \pm Q_2$ may be satisfied by choosing an appropriate combination of particle orientation and scattering directions. A trivial scheme that achieves this condition is the forward emission geometry, i.e., $\mathbf{q} = 0$. Further examination of Table I shows that Eq. (40) may also be satisfied approximately for arbitrary scattering directions under certain dimensional constraints, for example, the condition $a \ll \lambda$. Thus, another means of making a cylindrical particle appear chiral in terms of its nonlinear response is to make use of thin wires.

The employment of the two special geometrical configurations, i.e., forward scattering direction and thin wire dimensions, in order to imbue the cylinder with an effective chiral nonlinear optical response, is valid even for the case of arbitrary surface symmetry. For arbitrary emission directions and cylinder dimensions, it may be shown using Eqs. (27) and (29) that the effective susceptibility elements $\chi^{\text{eff}}_{x'y'z'}$ and $\chi^{\text{eff}}_{y'x'z'}$ become linear combinations of chiral and achiral surface susceptibility elements $\chi^{(2)}_{s,ijk}$ having the indices $\rho'\varphi'z'$, $\varphi'\rho'z'$, $\rho'\rho'z'$, $\varphi'\varphi'z'$, $x'y'z'$, and $y'x'z'$, with the last two terms originating from the end caps. Similarly $\chi^{\text{eff}}_{z'x'y'}$ becomes a linear combination of elements with indices $z'\rho'\varphi'$, $z'\rho'\rho'$, $z'\varphi'\varphi'$, and $z'x'y'$. By means of Eq. (36d) for forward emission, Eq. (40) is strictly obeyed, where $\chi^{\text{eff}}_{x'y'z'} = \chi^{\text{FE}}_{x'y'z'}$. By means of Eq. (38), together with Table III for thin wires, Eq. (40) is approximately satisfied, where $\chi^{\text{eff}}_{x'y'z'} \approx \chi^{\text{FE}}_{x'y'z'} \sin(Q_3 \Lambda a)/(Q_3 \Lambda a)$. In both cases, the geometrical chiral axis is established along the cylindrical axis and, in addition, the signal arises purely from the surface susceptibility components $\chi^{(2)}_{s,\rho'\varphi'z'}$ and $\chi^{(2)}_{s,\varphi'\rho'z'}$.

For comparison, consider a sphere of centrosymmetric medium with arbitrary surface symmetry. From Table II, the independent effective chiral susceptibility elements for the sphere also obey Eq. (40), with the geometrical effective chiral axis along the $\mathbf{q}$ direction. As in the case of the cylinder, the effective susceptibility element $\tilde{\chi}^{\text{eff}}_{x'y'z'}$ of the sphere is a linear combination of various surface chiral and achiral susceptibility elements. It comprises nonlinear susceptibility elements with the indices $\theta'\varphi'r'$, $\varphi'\theta'r'$, $r'\theta'\varphi'$, $\theta'\theta'\varphi'$, $\varphi'\theta'\theta'$, $\varphi'r'r'$, and $r'\varphi'r'$.

One significant consequence of the results above is that SHG may be used to probe chiral molecules adsorbed on a single cylindrical or spherical particle. Note that randomly oriented chiral molecules in solutions do not yield SHG whereas SFG is possible.[88–92] Thus, adsorption of chiral molecules onto a cylindrical or spherical particle of centrosymmetric medium may serve as a means to probe chiral molecules by SHG. There are, however, key differences between the cylinder and sphere as templates for studying chiral molecules. First, for a cylinder, the chiral axis may be established along the cylindrical axis by geometrical means, e.g., by forward emission or by use of thin wires at arbitrary scattering angles. For a sphere, the effective chiral axis is established along the **q** direction, a property that is true for *all* scattering angles and particle size. Second, for forward scattering, the cylinder's effective nonlinear chiral response depends on pure surface chiral elements. The nonlinear chiral response of the sphere, on the other hand, vanishes in the forward direction since in the limit as $\theta \rightarrow 0$, the vector **q**, which defines the geometrical chiral axis, becomes coplanar with the input-polarization vectors, which, for SHG, are degenerate. Note also that within the RGD approximation for the corresponding surface SFG chiral response from a sphere, the signal vanishes for collinear input beams in the forward direction; if the two input beams are noncollinear and their polarization vectors are orthogonal, the SFG signal in the "forward" direction ($\mathbf{q}=0$) becomes allowed.[54] At other scattering directions, the effective SH chiral response of the sphere arises from a mixture of chiral and achiral surface contributions. Third, for the case of small dimensions in the Rayleigh limit, or more generally, wires for the case of cylinders, the effective chiral nonlinear response from both particles depends on pure surface chiral elements: For the wire, $\chi^{\mathrm{eff}}_{x'y'z'} \propto (\chi^{(2)}_{s,\rho'\varphi'z'} - \chi^{(2)}_{s,\varphi'\rho'z'})$ [from Eq. (36d)], whereas for the sphere, the leading-order term is given by $\tilde{\chi}^{\mathrm{eff}}_{x'y'z'} \propto (-2\chi^{(2)}_{s,r'\theta'\varphi'} + \chi^{(2)}_{s,\theta'\varphi'r'} + \chi^{(2)}_{s,\varphi'\theta'r'})$ using Table II. Note that for the case of a general isotropic surface symmetry (without mirror plane), the leading-order element $\chi^{\mathrm{eff}}_{x'y'z'}$ of the cylinder is nonzero but the corresponding term for the sphere, $\tilde{\chi}^{\mathrm{eff}}_{x'y'z'}$, vanishes. From Table IV, the leading-order contribution of surface chirality for an isotropic surface yields the scaling $E^{(2\omega)} \sim A/\lambda^2$ and $\sim A^2/\lambda^4$, for the case of the cylinder and the sphere, respectively; i.e., in the Rayleigh limit for these two types of particles, the SH signal arising from chiral contributions is significantly weaker from spheres than from cylinders of comparable dimensions. Hence, in comparison to a sphere, the cylindrical particle may be a more suitable template for investigating surface chirality by SHG.

As we have shown above, the forward scattering direction may serve to isolate the chiral contribution by using appropriate particle and input-polarization directions. This property may find application in probing anisotropic particles of similar composition but having dissimilar topology, e.g., carbon nanotubes (CNTs), which exhibit chiral or achiral structural properties. Recently, theoretical studies have shown that the hyperpolarizability of a CNT may depend on its topological symmetry. For example within the dipole approximation, achiral and chiral CNTs yield zero and nonzero hyperpolarizabilities, respectively.[93] It has also been shown that torsional strain applied to *achiral* CNTs may generate a dipolar second-order nonlinear response.[65] Recently SHG from CNTs have been demonstrated experimentally, opening the possibility of investigating their topology and electronic structure by nonlinear optical scattering.[46,94,95]

As a final comment, it should be pointed out that the *achiral* effective nonlinear susceptibility elements of the cylinder might originate from both the achiral and chiral surface susceptibilities. For example, in the case of a general isotropic surface considered in Sec. III B above, $\chi^{\mathrm{eff}}_{x'z'x'}$ stems from two surface contributions: $\chi^{(2)}_{s,\parallel\perp\parallel}$ and $\chi^{(2)}_{s,\parallel//\perp}$. This observation of mixing chiral and achiral surface elements to yield an effective achiral nonlinear susceptibility is not unique to the case of centrosymmetric medium. In particular, inspection of Eq. (23) shows that for the noncentrosymmetric case, any effective nonlinear susceptibility element $\chi^{\mathrm{eff}}_{ijk}$ may arise from any of the bulk susceptibility elements $\chi^{(2)}_{ijk}$.

E. Linear-polarization dependence: isotropic vs anisotropic response

As we have shown above, the nonlinear response of an anisotropic structure, in terms of the number of the effective susceptibility elements and its source-emission characteristics, is considerably different from that of an isotropic system, i.e., a sphere of centrosymmetric medium. We now examine the polarization dependence of these two types of particles. Consider an input polarization described by $\hat{\boldsymbol{\epsilon}}_0 = \cos\psi\hat{\mathbf{x}} + \sin\psi\hat{\mathbf{y}}$, and $\mathcal{E}_i = M'_{ij}\epsilon_{0j}$ represents the polarization in the particle frame. We find that the nonlinear form factor component $p'_i = \chi^{\mathrm{eff}}_{ijk}\mathcal{E}_j\mathcal{E}_k$ is proportional to a linear combination of $\cos^2\psi$, $\sin^2\psi$, and $\cos\psi\sin\psi$. Consequently, the SHG power at any scattering direction may be expressed as $\mathcal{P}_\Omega = a_1\cos^4\psi + a_2\sin^4\psi + a_3\cos^2\psi\sin^2\psi + a_4\cos^3\psi\sin\psi + a_5\cos\psi\sin^3\psi$, where a_i are coefficients that depend on the scattering angles. This functional dependence has previously been presented for the case of SHG from spheres.[26] This equation may be expressed in terms of linearly independent functions $\{\cos(m\psi), \sin(m\psi)\}$ with $m=0,2,4$. Thus equivalently,

$$\mathcal{P}_\Omega = c_1 + c_2\cos 2\psi + c_3\cos 4\psi + c_4\sin 2\psi + c_5\sin 4\psi, \tag{41}$$

where the coefficients c_i depend on the scattering angles.

We now compare this result to a sphere comprised of centrosymmetric medium. It can be shown using Table II and Eq. (7) that if the effective nonlinear response is either purely achiral ($\tilde{\chi}^{\mathrm{eff}}_{x'y'z'}=0$) or purely chiral ($\tilde{\chi}^{\mathrm{eff}}_{z'z'z'} = \tilde{\chi}^{\mathrm{eff}}_{z'x'x'} = \tilde{\chi}^{\mathrm{eff}}_{x'z'x'} = 0$) the radiated power $\mathcal{P}_\Omega \propto |p_\theta|^2 + |p_\varphi|^2$, where p_θ and p_φ are the transverse components of **p** in the laboratory frame, may be written as

$$\mathcal{P}_\Omega = d_1 + d_2\cos 2(\psi-\varphi) + d_3\cos 4(\psi-\varphi), \tag{42}$$

where the coefficients d_i depend on θ. This result also emerges from the RGD discussion in Refs. 23 and 96 for the case of purely achiral isotropic surface contributions. The present calculation, however, includes all surface nonlinear susceptibility elements responsible for either the achiral or

chiral effective nonlinear response of the sphere. If $\varphi=0$ or $\pi/2$, or equivalently, if the input-polarization angle is referenced relative to the principal scattering planes, i.e., with respect to a plane parallel or perpendicular to the scattering plane, the overall polarization dependence of the scattered SH power from a sphere of centrosymmetric medium having either a pure achiral or chiral effective response may be written as

$$\mathcal{P}_\Omega = c_1 + c_2 \cos 2\psi + c_3 \cos 4\psi. \tag{43}$$

For the case of the cylinder with centrosymmetric medium, however, its general polarization response is given by Eq. (41) because of its intrinsic anisotropy. Hence, by comparison of Eqs. (41) and (43), the functional dependences $\sin 2\psi$ and $\sin 4\psi$ of the radiated power in Eq. (41) may be considered as terms associated with anisotropy, whether it pertains to structure or symmetry of the particle medium, or with mixed achiral and chiral response, for the case of a sphere of centrosymmetric medium. As a final note, for a sphere of centrosymmetric medium but with *arbitrary* surface response, which includes the chiral term $\tilde{\chi}^{\text{eff}}_{x'y'z'}$, the quantity $|\mathbf{p}|^2=|p_\theta|^2+|p_\varphi|^2+|p_r|^2=|\tilde{\chi}^{\text{eff}}_{ijk}\mathcal{E}_j\mathcal{E}_k|^2$ may be expressed as $|\mathbf{p}|^2=d_1'+d_2'\mathcal{E}_3^2+d_3'\mathcal{E}_3^4$, where d_i' are coefficients that depend on the scattering angles. For linear input polarization, $|\mathbf{p}|^2$ has the form given by Eq. (42).

IV. CONCLUSION

In this paper, we have developed the theory of SH scattering from finite cylinders of arbitrary symmetry within the RGD approximation. The nonlinear response of the particle may be described by the vector nonlinear form factor $\mathbf{p}$. For noncentrosymmetric medium, which exhibits bulk local response, the nonlinear form factor of the particle is expressed as a product of the linear optical form factor and the nonlinear susceptibility vector, i.e., $\mathbf{p}=f\boldsymbol{\chi}_0$, which is also valid for arbitrarily shaped particles. Furthermore, this simple relation implies that the various nonlinear optical susceptibility elements undergo the same scattering form factor f. For centrosymmetric medium, where the nonlinear optical response originates chiefly from the surface and the nonlocal bulk nonlinear polarization, the nonlinear form factor is more complex such that each nonlinear susceptibility element may experience different and multiple form factors. One commonality between these two types of particles, however, is that the nonlinear form factor may be expressed in terms of the effective susceptibility χ^{eff}_{ijk}. For a cylindrical particle of arbitrary material symmetry, there are in general 18 independent effective susceptibility tensors. This property is true even for the case of a cylinder comprising centrosymmetric medium whose local surface possesses a general isotropic symmetry. In contrast, a sphere with centrosymmetric medium of *arbitrary* surface symmetry possesses only four independent effective nonlinear susceptibility elements for SHG. This large difference in the number of effective susceptibility elements between these two systems indicates the significant influence of anisotropy that may stem from either the particle shape or symmetry of the medium, ensuing in an astonishingly complex nonlinear optical response of the cylindrical object in comparison to that of a sphere.

The validity of the RGD approximation has previously been tested and demonstrated experimentally with a high degree of success for the case of spheres of centrosymmetric media in SHG and SFG measurements even in the presence of slight index mismatch. We have applied this approximation to finite cylinders with the goal of bringing forth a lowest-order theory that provides suitable description and basic understanding of the nonlinear optical response of anisotropic structures. The consequences of this simple model are numerous and far reaching. Among those predictions of the theory include the largely anisotropic response of the SH field on the particle orientation and input-field polarization, its oscillatory dependence on the particle length, the directionality of the SH radiation, its rich scaling rules for small particles, and its distinctive chiral response. Clearly, much remains to be accomplished in developing a more general theoretical treatment that takes into account more realistic shapes and larger index contrast between that of the particle and the ambient media. Such endeavor is a daunting task as can be seen from the enormous amount of literature published on linear optical scattering alone. The rapid progress in nonlinear optical studies of particles, however, should provide further motivation for more rigorous theoretical treatments of nonlinear optical scattering which should, in turn, offer guidance for a new generation of particle characterization techniques as well as furnish better understanding and, perhaps, new approaches for important applications, such as SHG and SFG microscopy.

ACKNOWLEDGMENTS

I express my warmest gratitude to Alex de Beer, Tony Heinz, Sylvie Roke, and Jie Shan for useful comments and illuminating discussions.

APPENDIX A: NONLINEAR FORM FACTOR OF A CYLINDER

Here, we consider only the surface contribution from $\rho'=a$. A useful scheme that aids in evaluating the integral of Eq. (6) or more specifically Eq. (28) is to define the following parameters:[68]

$$Q_1 = Q \cos \mu, \tag{A1a}$$

$$Q_2 = Q \sin \mu. \tag{A1b}$$

Using Eqs. (A1a) and (A1b) and Eq. (15), we obtain

$$\mathbf{q}\cdot\mathbf{r}' = Q\rho' \cos(\varphi' - \mu) + Q_3 z'. \tag{A2}$$

Substitution of Eq. (A2) into the surface integral of Eq. (26) corresponding to the curved portion of the cylinder, $\rho'=a$, reduces Eq. (26) into Eq. (28) where

$$\mathbf{\Gamma} = \int_0^{2\pi} \vec{\boldsymbol{\chi}}_s^{(2)} : \hat{\boldsymbol{\epsilon}}_0 \hat{\boldsymbol{\epsilon}}_0 g(\varphi') d\varphi' \tag{A3}$$

and

$$g(\varphi') = \exp[i\delta_0 \cos(\varphi' - \mu)], \tag{A4}$$

with $\delta_0 = Qa$. In terms of the particle frame, $\mathbf{\Gamma} = \Gamma_i' \hat{x}_i'$. The quantity Γ_i' may be expressed as

$$\Gamma_i' = \int_0^{2\pi} \chi_{s,ijk}^{(2)} \mathcal{E}_j \mathcal{E}_k g(\varphi') d\varphi'$$

$$= \chi_{s,\alpha\beta\gamma}^{(2)} \mathcal{E}_j \mathcal{E}_k \int_0^{2\pi} A_{i\alpha} A_{j\beta} A_{k\gamma} g(\varphi') d\varphi', \tag{A5}$$

where $A_{i\alpha} = A_{i\alpha}(\varphi)$ is the transformation matrix element from cylindrical to Cartesian coordinates of the particle axis, i.e., $x_i' = A_{i\alpha} x_\alpha'$ with $i = (1,2,3)$ and $\alpha = (\rho', \varphi', z')$. The expression for Γ_i' has the form

$$I(\delta_0, \mu) = \int_0^{2\pi} u(\varphi') g(\varphi') d\varphi', \tag{A6}$$

where $u(\varphi') = \cos^m(\varphi') \sin^n(\varphi')$, $(m,n) = (0,1,2,3)$, and $0 \le (m+n) \le 3$. Equation (A6) may be further simplified by making the replacement $\varphi' \to \varphi' + \mu$ and using $u(\varphi') = u(\varphi' + 2\pi)$ to yield $I(\delta_0, \mu) = \int_0^{2\pi} u(\varphi' + \mu) g(\varphi' + \mu) d\varphi'$. After expanding $u(\varphi' + \mu)$, we collect the factors of the form $\cos^m(\varphi') \sin^n(\varphi')$, and the resulting integrals are expressed in terms of Bessel functions of orders ranging from 0 to 3. Specifically, we may define the following quantities

$$I_n = \int_0^{2\pi} K_n(\varphi') g(\varphi' + \mu) d\varphi', \tag{A7}$$

where

$$K_n(\varphi') = \begin{cases} 1, & n = 0 \\ \prod_{j=1}^{n} (A_j \cos \varphi' + B_j \sin \varphi'), & n > 0. \end{cases} \tag{A8}$$

Note that both I_n and K_n are implicit functions of the coefficients (A_j, B_j). The integrals I_n are evaluated to yield Eqs. (30a)–(30d).

APPENDIX B: NONLINEAR FORM FACTOR OF A SPHERE

1. Noncentrosymmetric medium

For the case of noncentrosymmetric medium, the nonlinear form factor is given by Eq. (16): $\mathbf{p} = f \boldsymbol{\chi}_0$, where the linear form factor may be expressed as

$$f = \left(\frac{9\pi}{2}\right)^{1/2} \frac{J_{3/2}(qa)}{(qa)^{3/2}}. \tag{B1}$$

$\boldsymbol{\chi}_0$ is given by Eq. (18), $q = 2K_1 \sin(\theta/2)$, and a is the radius of the sphere. Note here that one may extend the applicability of Eq. (16) to the case of an ellipsoidal particle by simply making the substitution $q \to [Q^2 + (Q_3 \Lambda)^2]^{1/2}$ in Eq. (B1),[69] using the definitions for Q, Q_3, and Λ, employed in Eq. (19) for the cylinder.

2. Centrosymmetric medium

For a particle comprised of centrosymmetric medium, the nonlinear form factor is calculated by assuming a particle reference frame described by the relation $x_i' = M_{ij}' x_j$. For the cylinder, the main axis and two axes orthogonal to it form a natural particle reference frame. For the sphere, a natural reference frame may be defined in terms of the direction $\mathbf{q}$. In particular, one may set $\hat{\mathbf{z}}' = \mathbf{q}/q$. The coordinates x' and y' may be defined according to the relation $x_i' = M_{ij}' x_j$, where $M_{ij}' = M_{ij}(\varphi, \theta/2 - \pi/2, 0)$ and M_{ij} is an element of $\mathbf{M}$ defined in Eq. (9). The matrix $\mathbf{M}'$ transforms the input-polarization vector component ϵ_{0i} into the polarization component $\mathcal{E}_i$ in the particle frame ($\mathcal{E}_i = M_{ij}' \epsilon_{0j}$), and converts the calculated nonlinear form factor in the particle frame back to the corresponding laboratory frame quantity according to Eq. (31). Making use of the particle reference frame and the source coordinates described by $\{\hat{\mathbf{r}}', \hat{\boldsymbol{\theta}}', \hat{\boldsymbol{\varphi}}'\}$ in spherical coordinate system, one may calculate the surface nonlinear form factor given by $\mathbf{p}_s = (1/V) \int \vec{\vec{\chi}}_s^{(2)} : \hat{\boldsymbol{\epsilon}}_0 \hat{\boldsymbol{\epsilon}}_0 \delta(r' - a) \exp(i\mathbf{q} \cdot \mathbf{r}') d\mathbf{r}'$, which becomes

$$\mathbf{p}_s = \frac{3}{4\pi a} \int_0^{2\pi} \int_0^{\pi} \vec{\vec{\chi}}_s^{(2)} : \hat{\boldsymbol{\epsilon}}_0 \hat{\boldsymbol{\epsilon}}_0 \tilde{g}(\theta') \sin(\theta') d\theta' d\varphi', \tag{B2}$$

where $\delta = qa = 2K_1 a \sin(\theta/2)$ and $\tilde{g}(\theta') = \exp[i\delta \cos(\theta')]$. In the particle frame, the component $p_{s,i}'$ of the surface nonlinear form factor becomes

$$p_{s,i}' = \frac{3}{4\pi a} \int_0^{2\pi} \int_0^{\pi} \chi_{s,ijk}^{(2)} \mathcal{E}_j \mathcal{E}_k \tilde{g}(\theta') \sin(\theta') d\theta' d\varphi'$$

$$= \frac{3}{4\pi a} \chi_{s,\alpha\beta\gamma}^{(2)} \mathcal{E}_j \mathcal{E}_k \int_0^{2\pi} \int_0^{\pi} B_{i\alpha} B_{j\beta} B_{k\gamma} \tilde{g}(\theta') d\theta' d\varphi', \tag{B3}$$

where $B_{i\alpha} = B_{i\alpha}(\theta, \varphi)$ is the transformation matrix element from spherical to Cartesian coordinates of the particle axis, i.e., $x_i' = B_{i\alpha} x_\alpha'$, where $i = (1,2,3)$ and $\alpha = (\theta', \varphi', r')$. In Eq. (B3), we have implicitly made the assumption that the local surface nonlinear response is anisotropic and the nonlinear susceptibility elements, $\chi_{s,\alpha\beta\gamma}^{(2)}$, where the indices α, β, and γ refer to the spherical coordinates, are constants within the spherical coordinate reference frame of the particle.

The contribution from the bulk, $\mathbf{p}_b$, is given by

$$\mathbf{p}_b = i\gamma (\hat{\boldsymbol{\epsilon}}_0 \cdot \hat{\boldsymbol{\epsilon}}_0) f \mathbf{q}, \tag{B4}$$

which was derived in a similar fashion as in Eq. (25) but with f given by Eq. (B1). In the particle reference frame,

$$p_{b,i}' = i\gamma \mathcal{E}_j \mathcal{E}_j f q \delta_{iz'}. \tag{B5}$$

Inspection of Eqs. (B3) and (B5) shows that the total component of the nonlinear form factor, i.e., $p_i' = p_{s,i}' + p_{b,i}'$, may be written as

$$p_i' = \tilde{\chi}_{ijk}^{\text{eff}} \mathcal{E}_j \mathcal{E}_k, \tag{B6}$$

where the elements of the effective susceptibility may be

expressed as $\tilde{\chi}_{ijk}^{\mathrm{eff}}=\Sigma_n \tilde{\kappa}_{ijk,n} J_{(n+1)/2}(\delta)/\delta^{(n+1)/2}$ are given in Table II. If we consider only the achiral contributions to the isotropic surface response corresponding to the surface susceptibility elements $\{\chi_{s,\perp\perp\perp}^{(2)}, \chi_{s,\perp\parallel\parallel}^{(2)}, \chi_{s,\parallel\perp\parallel}^{(2)}\}$, we obtain the RGD expression for the SH field in Ref. 23 (see comments in Ref. 96). For SFG from spheres of arbitrary surface symmetry, the effective susceptibility has been calculated and presented in Ref. 54.

[1] S. K. Kurtz and T. T. Perry, J. Appl. Phys. **39**, 3798 (1968).
[2] S. Brasselet, V. Le Floc'h, F. Treussart, J. F. Roch, J. Zyss, E. Botzung-Appert, and A. Ibanez, Phys. Rev. Lett. **92**, 207401 (2004).
[3] E. Delahaye, N. Tancrez, T. Yi, I. Ledoux, J. Zyss, S. Brasselet, and R. Clément, Chem. Phys. Lett. **429**, 533 (2006).
[4] L. Bonacina, Y. Mugnier, F. Courvoisier, R. Le Dantec, J. Extermann, Y. Lambert, V. Boutou, C. Galez, and J.-P. Wolf, Appl. Phys. B: Lasers Opt. **87**, 399 (2007).
[5] J. P. Long, B. S. Simpkins, D. J. Rowenhorst, and P. E. Pehrsson, Nano Lett. **7**, 831 (2007).
[6] T. F. Heinz, in *Nonlinear Surface Electromagnetic Phenomena*, edited by H. Ponath and G. Stegeman (Elsevier, Amsterdam, 1991), p. 353.
[7] J. F. McGilp, Prog. Surf. Sci. **49**, 1 (1995).
[8] K. B. Eisenthal, Chem. Rev. (Washington, D.C.) **96**, 1343 (1996).
[9] G. Lüpke, Surf. Sci. Rep. **35**, 75 (1999).
[10] M. C. Downer, B. S. Mendoza, and V. I. Gavrilenko, Surf. Interface Anal. **31**, 966 (2001).
[11] J. I. Dadap and T. F. Heinz, in *Encyclopedia of Modern Optics*, edited by Robert D. Guenther, Duncan G. Steel, and Leopold Bayvel (Elsevier, Oxford, 2004), Vol. 5, p. 134.
[12] M. B. Raschke and Y. R. Shen, Curr. Opin. Solid State Mater. Sci. **8**, 343 (2004).
[13] H. Wang, E. C. Y. Yan, E. Borguet, and K. B. Eisenthal, Chem. Phys. Lett. **259**, 15 (1996).
[14] L. Schneider and W. Peukert, Part. Part. Syst. Charact. **23**, 351 (2006).
[15] K. B. Eisenthal, Chem. Rev. (Washington, D.C.) **106**, 1462 (2006).
[16] P. J. Campagnola and L. M. Loew, Nat. Biotechnol. **21**, 1356 (2003).
[17] W. R. Zipfel, R. M. Williams, and W. W. Webb, Nat. Biotechnol. **21**, 1369 (2003).
[18] J. Mertz, Curr. Opin. Neurobiol. **14**, 610 (2004).
[19] C. K. Sun, Adv. Biochem. Eng./Biotechnol. **95**, 17 (2005).
[20] R. C. Jin, J. E. Jureller, H. Y. Kim, and N. F. Scherer, J. Am. Chem. Soc. **127**, 12482 (2005).
[21] B. K. Canfield, H. Husu, J. Laukkanen, B. Bai, M. Kuittinen, J. Turunen, and M. Kauranen, Nano Lett. **7**, 1251 (2007).
[22] J. I. Dadap, J. Shan, K. B. Eisenthal, and T. F. Heinz, Phys. Rev. Lett. **83**, 4045 (1999).
[23] J. I. Dadap, J. Shan, and T. F. Heinz, J. Opt. Soc. Am. B **21**, 1328 (2004).
[24] J. Shan, J. I. Dadap, I. Stiopkin, G. A. Reider, and T. F. Heinz, Phys. Rev. A **73**, 023819 (2006).
[25] E. C. Hao, G. C. Schatz, R. C. Johnson, and J. T. Hupp, J. Chem. Phys. **117**, 5963 (2002).
[26] J. Nappa, G. Revillod, I. Russier-Antoine, E. Benichou, C. Jonin, and P. F. Brevet, Phys. Rev. B **71**, 165407 (2005).
[27] G. Bachelier, I. Russier-Antoine, E. Benichou, C. Jonin, and P. Brevet, J. Opt. Soc. Am. B **25**, 955 (2008).
[28] M. Finazzi, P. Biagioni, M. Celebrano, and L. Duò, Phys. Rev. B **76**, 125414 (2007).
[29] M. L. Sandrock, C. D. Pibel, F. M. Geiger, and C. A. Foss, J. Phys. Chem. B **103**, 2668 (1999).
[30] E. C. Y. Yan and K. B. Eisenthal, J. Phys. Chem. B **104**, 6686 (2000).
[31] J. C. Johnson, H. Yan, R. D. Schaller, P. B. Petersen, P. Yang, and R. J. Saykally, Nano Lett. **2**, 279 (2002).
[32] A. Podlipensky, J. Lange, G. Seifert, H. Graener, and I. Cravetchi, Opt. Lett. **28**, 716 (2003).
[33] J. Nappa, G. Revillod, J. P. Abid, I. Russier-Antoine, C. Jonin, E. Benichou, H. H. Girault, and P. F. Brevet, Faraday Discuss. **125**, 145 (2004).
[34] T. Kitahara, A. Sugawara, H. Sano, and G. Mizutani, J. Appl. Phys. **95**, 5002 (2004).
[35] C. C. Neacsu, G. A. Reider, and M. B. Raschke, Phys. Rev. B **71**, 201402(R) (2005).
[36] B. K. Canfield, S. Kujala, K. Laiho, K. Jefimovs, T. Vallius, J. Turunen, and M. Kauranen, J. Nonlinear Opt. Phys. Mater. **15**, 43 (2006).
[37] S. W. Chan, R. Barille, J. M. Nunzi, K. H. Tam, Y. H. Leung, W. K. Chan, and A. B. Djurisic, Appl. Phys. B: Lasers Opt. **84**, 351 (2006).
[38] M. D. McMahon, R. Lopez, R. F. Haglund, E. A. Ray and P. H. Bunton, Phys. Rev. B **73**, 041401(R) (2006).
[39] R. Prasanth, L. K. van Vugt, D. A. M. Vanmaekelbergh, and H. C. Gerritsen, Appl. Phys. Lett. **88**, 181501 (2006).
[40] J. Brewer, M. Schiek, A. Lützen, K. Al-Shamery, and H.-G. Rubahn, Nano Lett. **6**, 2656 (2006).
[41] S. Kujala, B. K. Canfield, M. Kauranen, Y. Svirko, and Jari Turunen, Phys. Rev. Lett. **98**, 167403 (2007).
[42] C. Hubert, L. Billot, P.-M. Adam, R. Bachelot, P. Royer, J. Grand, D. Gindre, K. D. Dorkenoo, and A. Fort, Appl. Phys. Lett. **90**, 181105 (2007).
[43] M. Zavelani-Rossi, M. Celebrano, P. Biagioni, D. Polli, M. Finazzi, L. Duò, G. Cerullo, M. Labardi, M. Allegrini, J. Grand, and P.-M. Adam, Appl. Phys. Lett. **92**, 093119 (2008).
[44] S. W. Liu, H. J. Zhou, A. Ricca, R. Tian, and M. Xiao, Phys. Rev. B **77**, 113311 (2008).
[45] V. Barzda, R. Cisek, T. L. Spencer, U. Philipose, H. E. Ruda, and A. Shik, Appl. Phys. Lett. **92**, 113111 (2008).
[46] H. M. Su, J. T. Ye, Z. K. Tang, and K. S. Wong, Phys. Rev. B **77**, 125428 (2008).
[47] G. S. Agarwal and S. S. Jha, Solid State Commun. **41**, 499 (1982).
[48] J. P. Dewitz, W. Hübner, and K. H. Bennemann, Z. Phys. D: At., Mol. Clusters **37**, 75 (1996).
[49] J. Martorell, R. Vilaseca, and R. Corbalán, Phys. Rev. A **55**, 4520 (1997).

[50] V. L. Brudny, B. S. Mendoza, and W. L. Mochán, Phys. Rev. B **62**, 11152 (2000).
[51] W. L. Mochán, J. A. Maytorena, B. S. Mendoza, and V. L. Brudny, Phys. Rev. B **68**, 085318 (2003).
[52] S. Roke, W. G. Roeterdink, J. E. G. J. Wijnhoven, A. V. Petukhov, A. W. Kleyn, and M. Bonn, Phys. Rev. Lett. **91**, 258302 (2003).
[53] S. Roke, M. Bonn, and A. V. Petukhov, Phys. Rev. B **70**, 115106 (2004).
[54] A. G. F. de Beer and S. Roke, Phys. Rev. B **75**, 245438 (2007).
[55] Y. Pavlyukh and W. Hübner, Phys. Rev. B **70**, 245434 (2004).
[56] S. Roth and I. Freund, J. Chem. Phys. **70**, 1637 (1979).
[57] S. Roth and I. Freund, Biopolymers **20**, 1271 (1981).
[58] C. I. Valencia, E. R. Mendez, and B. S. Mendoza, J. Opt. Soc. Am. B **20**, 2150 (2003).
[59] C. I. Valencia, E. R. Mendez, and B. S. Mendoza, J. Opt. Soc. Am. B **21**, 36 (2004).
[60] H. E. Ruda and A. Shik, J. Appl. Phys. **101**, 034312 (2007).
[61] J. Zhu, Nanotechnology **18**, 225702 (2007).
[62] L. Cao, N. C. Panoiu, and R. M. Osgood, Phys. Rev. B **75**, 205401 (2007).
[63] G. Y. Guo, K. C. Chu, D.-S. Wang, and C.-G. Duan, Phys. Rev. B **69**, 205416 (2004).
[64] G. Y. Guo and J. C. Lin, Phys. Rev. B **72**, 075416 (2005).
[65] J. Zhou, H.-M. Weng, G. Wu, and J.-M. Dong, Appl. Phys. Lett. **89**, 013102 (2006).
[66] M. Kerker, *The Scattering of Light and Other Electromagnetic Radiation* (Academic, New York, 1969).
[67] H. C. van de Hulst, *Light Scattering by Small Particles* (Dover, New York, 1981).
[68] C. F. Bohren and D. R. Huffman, *Absorption and Scattering of Light by Small Particles* (Wiley, New York, 1983).
[69] P. J. Wyatt, Appl. Opt. **7**, 1879 (1968).
[70] L. D. Cohen, R. D. Haracz, A. Cohen, and C. Acquista, Appl. Opt. **22**, 742 (1983).
[71] P. J. Wyatt, Anal. Chim. Acta **272**, 1 (1993).
[72] J. D. Klett and R. A. Sutherland, Appl. Opt. **31**, 373 (1992).
[73] N. Yang, W. E. Angerer, and A. G. Yodh, Phys. Rev. Lett. **87**, 103902 (2001).
[74] S. H. Jen and H. L. Dai, J. Phys. Chem. B **110**, 23000 (2006).
[75] J. D. Jackson, *Classical Electrodynamics*, 2nd ed. (Wiley, New York, 1975).
[76] L. Moreaux, O. Sandre, and J. Mertz, J. Opt. Soc. Am. B **17**, 1685 (2000).
[77] P. Stoller, K. M. Reiser, P. M. Celliers, and A. M. Rubenchik, Biophys. J. **82**, 3330 (2002).
[78] D. A. Kleinman, Phys. Rev. **126**, 1977 (1962).
[79] P. J. Campagnola, A. C. Millard, M. Terasaki, P. E. Hoppe, C. J. Malone, and W. A. Mohler, Biophys. J. **81**, 493 (2002).
[80] P. Stoller, P. M. Celliers, K. M. Reiser, and A. M. Rubenchik, Appl. Opt. **42**, 5209 (2003).
[81] R. M. Williams, W. R. Zipfel, and W. W. Webb, Biophys. J. **88**, 1377 (2005).
[82] M. Nuriya, J. Jiang, B. Nemet, K. B. Eisenthal, and R. Yuste, Proc. Natl. Acad. Sci. U.S.A. **103**, 786 (2006).
[83] Y. Fu, H. Wang, R. Shi, and J.-X. Chen, Biophys. J. **92**, 3251 (2007).
[84] J. A. Palero, H. S. de Bruijn, A. van der Ploeg van den Heuvel, H. J. C. M. Sterenborg, and H. C. Gerritsen, Biophys. J. **93**, 992 (2007).
[85] I. Rocha-Mendoza, D. R. Yankelevich, M. Wang, K. M. Reiser, C. W. Frank, and A. Knoesen, Biophys. J. **93**, 4433 (2007).
[86] J. E. Sipe, V. Mizrahi, and G. I. Stegeman, Phys. Rev. B **35**, 9091 (1987).
[87] V. L. Brudny and W. L. Mochan, Phys. Status Solidi A **175**, 183 (1999).
[88] S. Sioncke, T. Verbiest, and A. Persoons, Mater. Sci. Eng. R. **42**, 115 (2003).
[89] G. J. Simpson, ChemPhysChem **5**, 1301 (2004).
[90] P. Fischer and F. Hache, Chirality **17**, 421 (2005).
[91] M. A. Belkin and Y. R. Shen, Int. Rev. Phys. Chem. **24**, 257 (2005).
[92] N. Ji and Y.-R. Shen, Chirality **18**, 146 (2006).
[93] L. De Dominicis, R. Fantoni, S. Botti, L. S. Asilyan, R. Ciardi, A. Fiori, and R. Appolloni, Laser Phys. Lett. **1**, 172 (2004).
[94] L. De Dominicis, S. Botti, L. S. Asilyan, R. Ciardi, R. Fantoni, M. L. Terranova, A. Fiori, S. Orlanducci, and R. Appolloni, Appl. Phys. Lett. **85**, 1418 (2004).
[95] D. A. Akimov, M. V. Alfimov, S. O. Konorov, A. A. Ivanov, S. Botti, A. A. Podshivalov, R. Ciardi, L. De Dominicis, L. S. Asilyan, R. Fantoni, and A. M. Zheltikov, J. Exp. Theor. Phys. **98**, 220 (2004).
[96] Here we take the opportunity to correct two typographical errors in the SH RGD formula presented in Reference and Notes no. 106 in Ref. 23: (1) The quantity δ is given by $\delta = 2K_1 a \sin(\theta/2)$, and (2) the expression for the SH field $\mathbf{E}^{(2\omega)}$ has to be multiplied by a factor of $1/\delta$.